MER-0056-FM-9043-393

BRIDGE FATIGUE MONITORING DEVICE

D. Thomson
G. Samavedam
Foster-Miller, Inc.
350 Second Avenue
Waltham, MA 02154

Final Report
Contract No. DAAK70-89-C-0056

November 1990

Prepared for:

U.S. Army Troop Support Command
Belvoir Procurement Division
Ft. Belvoir, VA 22060-5606

MER-0056-FM-9043-393

BRIDGE FATIGUE MONITORING DEVICE

D. Thomson
G. Samavedam
Foster-Miller, Inc.
350 Second Avenue
Waltham, MA 02154

Final Report
Contract No. DAAK70-89-C-0056

November 1990

Prepared for:

U.S. Army Troop Support Command
Belvoir Procurement Division
Ft. Belvoir, VA 22060-5606

252.227-7036 CERTIFICATION OF TECHNICAL DATA CONFORMITY (MAY 1987)

a. All technical data delivered under this contract shall be accompanied by the following written certification:

The Contractor, Foster-Miller, Inc., hereby certifies that, to the best of its knowledge and belief, the technical data delivered herewith under Contract No. DAAK70-89-C-0056, CDRL A002 is complete, accurate, and complies with all requirements of the contract.

Date 25 September 1989

Name and Title of Certifying Official

Gopal Samavedam; Program Manager

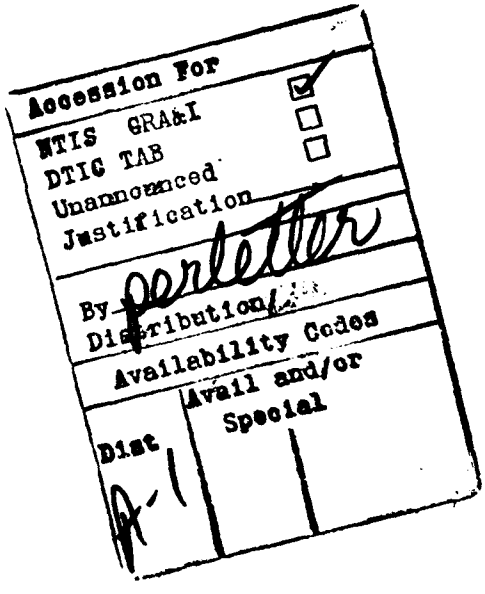

TABLE OF CONTENTS

TABLE OF CONTENTS (Continued)

LIST OF ILLUSTRATIONS

LIST OF ILLUSTRATIONS (Continued)

LIST OF TABLES

1. PROGRAM SUMMARY

This program involved development and design of the Twin Coupon Fatigue Monitoring System and the concept validation in the laboratory. The tasks are defined in the contract DAAK70-89-C-0056. The Technical Program Officer at Ft. Belvoir, VA is Brian Hombeck. The work performed in each task is summarized below and described in detail in later sections.

Task 1 - Bridge Fatigue Life Definition

The Armored Vehicle Launched Bridge (AVLB) was selected as the basis for the design of the Fatigue Life Indicator (FLI) system. The Directorate of Combat Engineering at Ft. Belvoir, VA provided static test data and design life criteria for the bridge. No fatigue data was available for this bridge.

Task 2 - Coupon Analysis and Design

The twin coupons were initially designed for a wide stress range. In consideration of the fact that the load rating of the AVLB may be upgraded and that this FLI system may be later applied to higher stress bridges such as the Light Assault Bridge (LAB), initial material selection and sizing calculations were made at 24 Ksi. Later in the program, the initial crack lengths were adjusted to better suit field proof-of-concept testing on the AVLB.

Task 3 - Coupon Attachment

Several attachment techniques were reviewed and tested. The primary selection criteria was for the attachment technique to be sufficient for the laboratory proof-of-concept testing. A bolted joint was found to be simplest. A bonded technique has also been conceived and needs to be demonstrated in field applications.

Task 4 - Coupon Manufacturing

A method of producing "identical" precracked coupons was developed. This was of primary importance as the system's accuracy depends on the initial condition of the coupons. It was also shown that the coupons could be cyclically loaded to the required initial crack lengths.

Task 5 - Laboratory Proof-of-Concept

A total of 11 full assembly tests were conducted. These tests proved both the repeatability of the FLI system. The accuracy was established when compared to the known loading. Laboratory crack length measurement was made with a graduated microscope to a resolution of 0.002 in.

Task 6 - Field Test Coupon Preparation

Five sets of twin coupons were prepared each with an initial half crack length of 0.250 in. This was defined as the optimum initial crack length for the expected stress levels of the AVLB. Recommendations were made for field measurement and coupon protection. The required hardware for the attachment method was also included with these coupons.

Computer Software

A basic program (FMFLCALC) was developed to deduce the stress histograms from the measured crack lengths. This program was successfully tested for the laboratory applied loads and cycles on tested coupons. Documentation of this program is presented in this report.

2. INTRODUCTION

Military bridges are designed to carry substantial loads, yet must be easily moved and quickly erected in tactical field situations. This requires a modular design utilizing high strength-to-weight ratio materials. To further enhance portability, bridge weight is minimized by sacrificing ultimate and fatigue strength in a tradeoff with useful life. The final result is a lightweight bridge with a useful, but limited, life.

These bridges must be removed from service before their useful life is exceeded. This poses a serious problem, as individual bridges are used at various locations over different spans with generally undefined traffic patterns. At present, there is no accurate way to determine when a given bridge is approaching its useful life and needs to be removed from service. Therefore, there is a need for a technique for measuring the actual service that the bridge has seen and for relating that service to the predicted fatigue life.

There are several fatigue-critical areas in military bridges such as welds, bolt or rivet holes and hinges. Vehicles crossing over the bridge produce a single major stress cycle at any point under consideration, with superimposed vibrational stress, as in Figure 2-1. As is currently assumed in the highway bridges (6,7), the vibratory stress is negligible, hence, the number of fatigue causing stress cycles is equal to the number of vehicle crossings.

Bridge fatigue damage requires an appropriate quantitative evaluation. The fatigue damage can be seen in the form of fatigue cracks emanating from rivet holes, hinges, weldments and other fatigue critical locations. Hidden cracks such as under rivet heads may also exist, which may need NDI. Although crack size can be used as a measure of fatigue life consumed, their inspection in field service may not be practical. However, knowledge of maximum permissible crack size in the bridge should be established through fracture mechanics and damage tolerance analysis. This will determine the maximum possible fatigue life for the bridge structure before a major catostrophic fracture failure will occur. With this information, a fatigue device can be designed to monitor the percent of total fatigue life consumed at any given instant in service.

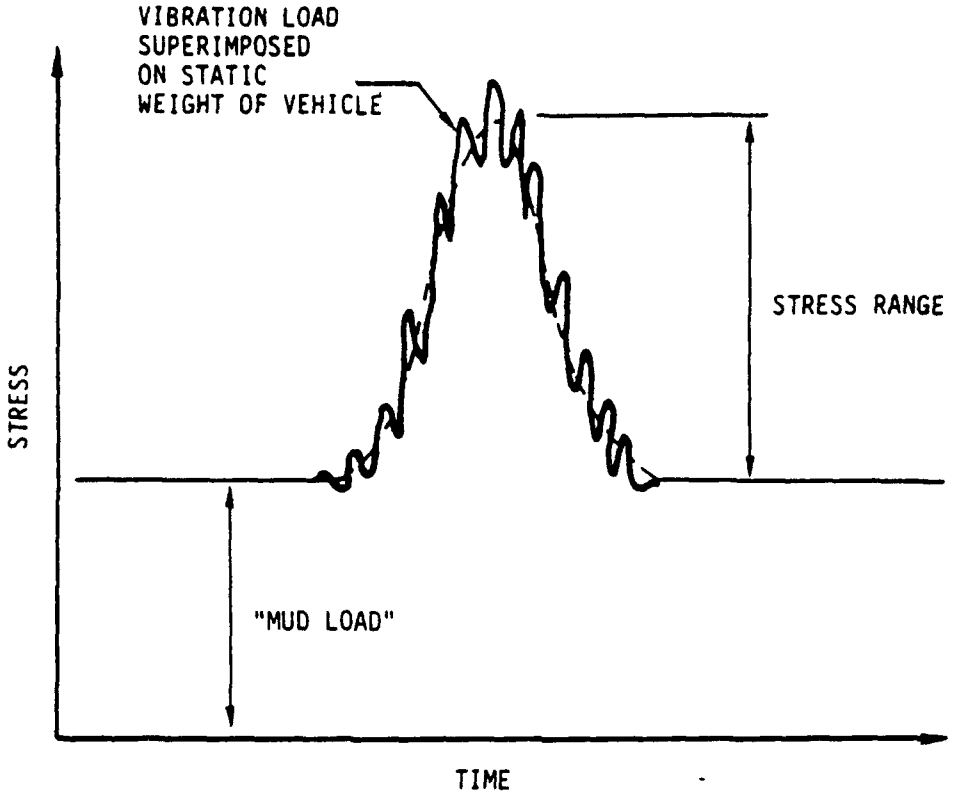

Figure 2-1. Stress in Bridge due to Passage of Vehicle

It should be noted that although at present the Army bridges are designed for a prescribed number of vehicle crossings at a given load level, there is no reason to believe that the fatigue life will be fully consumed within these crossings. It may be economic to extend the bridge life beyond the design value or it may be safer to remove the bridge from service in a timely manner if the life is found to be shorter than the design life. The fatigue life monitoring device should be useful in either situation.

The ideal requirements of the fatigue monitoring device are:

- It shall separate out the load levels and cycle number, i.e., it should monitor the load histogram. This will facilitate determination of fatigue life anywhere in the bridge, not merely at the particular location where the device is attached or mounted on the bridge. The vehicle crossing history is also useful to the Army in their battle logistics.

- It shall not require empirical correlation or field calibration.
- It shall be rugged and easily protectable from weather.
- It shall be passive, not requiring battery source, complex signal conditioning and electronics which is a problem with strain gauge type devices.
- It should be low in initial and maintenance costs.
- It should be usable by untrained personnel.

A fatigue monitoring device suitable for the Army use has been proposed and validated in this report.

3. PROPOSED CONCEPT

3.1 Background

An early concept of fatigue life monitoring system proposed by Samavedam to the U.S. Army in 1981, used prenotched fatigue coupons which would act like fuses and fail completely at a given fractional life of the structure to which the coupons would be attached. By varying the notch geometry, appropriate levels of stress concentration at the notch can be generated to yield desired fractional life of the coupons.

A disadvantage of the forgoing fatigue coupon approach is that it is dependent on the fatigue crack *initiation* phenomenon. It is well-known in the literature that the number of cycles required for the fatigue crack initiation will vary even among "identical" specimens. Hence, significant scatter will result in this approach.

In contrast to the concept dependent on crack initiation, concepts utilizing crack *growth* phenomenon are reliable and this has been adopted in the Twin Coupon approach, originally proposed by Samavedam in 1988 to the U.S. Army. Furthermore, the Twin Coupon technique can separate the stress levels and the number of cycles experienced by the parent structure to which the coupons will be attached. This is a considerable advantage over the simplistic fatigue coupon fuses referred to previously.

The Twin Coupon method works on the well-established principle of Fracture Mechanics. Figure 3-1 shows the crack growth rate versus the stress intensity factor at the crack tip. Region I represents a combination of crack initiation and microcrack development period. Region *II* represents the well-known Paris region in which the crack growth law is well-defined and *linear*. The Twin Coupons are designed to operate essentially in the Region II. This is accomplished by precracking the coupons and removing the uncertainty associated with crack initiation in Region I.

3.2 Twin Coupon Concept Basis

The concept utilizes precracked fatigue coupons, rigidly fastened to any bridge structural member under tension. The attachment makes the coupons experience the same number of

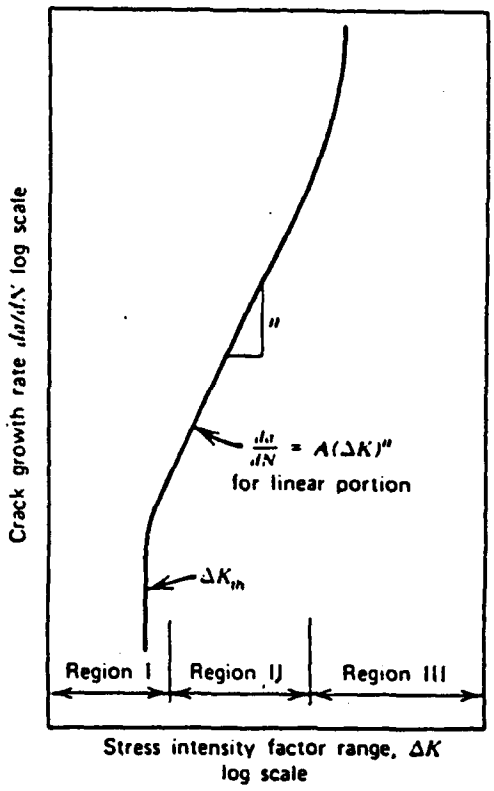

Figure 3-1. Schematic Sigmoidal Behavior of Fatigue Crack Growth versus ΔK

cycles and proportional stress levels as the structural member. With rational coupon design, using fracture mechanics theory for crack propagation, the crack length at any instant can be used as a measure of the consumed fatigue life of the bridge structural element under evaluation. (It is not necessary to mount the coupon on the particular bridge element of concern). Using twin coupons of different materials, mounted at the same location, and measuring both crack lengths from time to time, the stress histograms (stress versus cycles) can be deduced. This is the significant advantage over single coupon designs. Since two coupons of different materials are used, both unknowns (stress and cycles) can be determined by measuring the two crack lengths. In single coupons, one of these quantities must be known in order to determine the other. The stress at the coupon location can then be used to determine the stress at other fatigue critical locations. A typical coupon is shown in Figure 3-2.

To show how the histograms can be deduced using the concept let us assume that we have two coupons with different crack lengths and of different materials. The two coupons will be respectively represented by suffixes 1 and 2. The equation for crack propagation in coupon No.1 is:

$$\frac{da_1}{dN} = C_1 \Delta K_1^{\ n_1} \qquad (3\text{-}1)$$

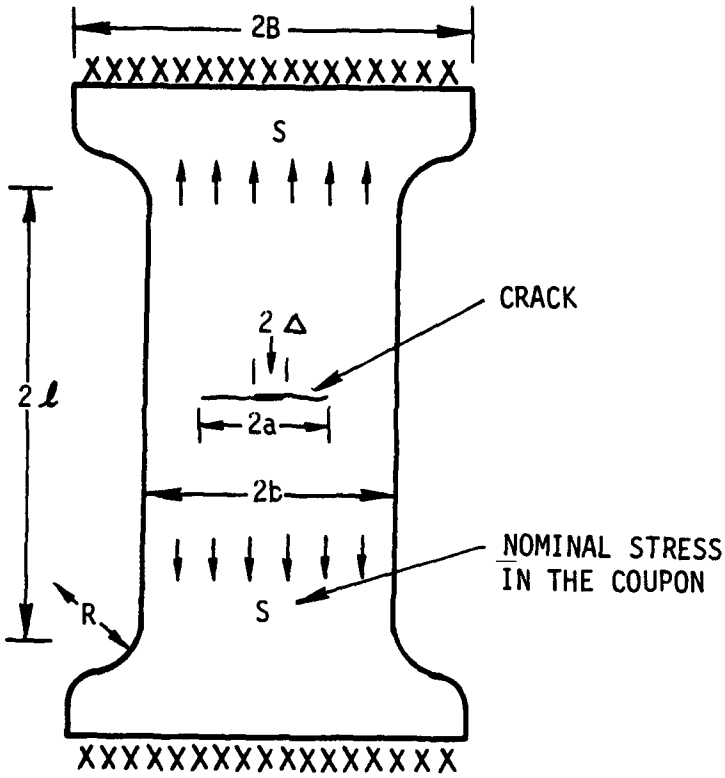

Figure 3-2. Precracked Fatigue Coupon Geometry

For simplicity, we use the expression for K as that of the infinite plate. The finite plate expressions do not pose special problems.

$$\Delta K_1 = \Delta_1 \sigma_1 \sqrt{\pi\ a_1} \tag{3-2}$$

For coupon No. 2 the equation is:

$$\frac{da_2}{dN} = C_2 \Delta K_2^{\ n_2} \tag{3-3}$$

$$\Delta K_2 = \Delta \sigma_2\ \sqrt{\pi\ a_2} \tag{3-4}$$

The two coupons will have equal strains, and thus for coupon materials with the same moduli, we have $\Delta\sigma_1 = \Delta\sigma_2$.

The number of cycles (N) is defined by integrating Equation 3-1.

$$N = \frac{a^{1-n/2} - a_i^{1-n/2}}{c\Delta\sigma^{n}\pi^{n/2}\left(1-n/2\right)} \tag{3-5}$$

Since the stress cycle ($\Delta\sigma$) and the number of cycles (N) is the same for both coupons, $\Delta\sigma$ is defined from Equation 3-5 as:

$$\frac{a_1^{1-\frac{n_1}{2}} - a_{1_i}^{1-\frac{n_1}{2}}}{c_1\Delta\sigma^{n_1}\pi^{\frac{n_1}{2}}\left(1-\frac{n_1}{2}\right)} = \frac{a_2^{1-\frac{n_2}{2}} - a_{2_i}^{1-\frac{n_2}{2}}}{c_2\Delta\sigma^{n_2}\pi^{\frac{n_2}{2}}\left(1-\frac{n_2}{2}\right)} \tag{3-6}$$

or

$$\Delta\sigma = \left[\frac{c_2\pi^{\frac{n_2}{2}}\left(1-\frac{n_2}{2}\right)\left(a_1^{1-\frac{n_1}{2}} - a_{1_i}^{1-\frac{n_1}{2}}\right)}{c_1\pi^{\frac{n_1}{2}}\left(1-\frac{n_1}{2}\right)\left(a_2^{1-\frac{n_2}{2}} - a_{2_i}^{1-\frac{n_2}{2}}\right)}\right]^{\frac{1}{n_1-n_2}} \tag{3-7}$$

Using this equation, the stress cycle, and consequently the number of cycles, may be calculated. This calculated stress cycle is a weighted average of all of the vehicle crossings (N). This loading history may then be used to calculate the fatigue life consumed.

The fatigue of smooth metals is evaluated from the S-N curve determined experimentally. The fatigue life in cycles at a stress range of $\Delta\sigma$ is given by

$$N = \beta/\Delta\sigma^{\alpha} \tag{3-8}$$

where α, β are material constants. If the structure is subjected to N_1 cycles at this range, the fraction of life consumed, f, is given by

$$f = N_1/N \tag{3-9}$$

For the military bridge, if $\Delta\sigma_i$ represents the stress range at the i-th vehicle crossing, using the cumulative damage rule of Miner (1), it can be shown that the fractional life consumed for the total number of crossings N is

$$f = \frac{1}{\beta} \sum_{i=1}^{N} \Delta\sigma_i^{\alpha} \tag{3-10}$$

3.3 Computer Program for Stress Histogram

A BASIC computer program was written to deduce the loading history based on the two crack lengths. Since the initial crack lengths have been defined for the contract deliverable coupons, this program requires input of only the current crack lengths from the two coupons. However, incremental loading histories may be deduced if the initial crack lengths of the increment are known. For the purposes of analyzing the test results presented in this report, this program also required input of the initial crack lengths.

The program written uses the initial and final crack lengths to calculate the stress cycle using Equation 3-7. For this first calculation, the below transition constants for 6061-T6 are used. A check is then made to determine if transition has been exceeded for the stress level. If transition is exceeded, the stress level above transition is calculated using Equation 3-7 and the above transition constants for 6061-T6. The two calculated stress levels are compared and an iteration process followed until these stress levels are equal. The total number of cycles at this stress level is then calculated using Equation 3-5. The stress cycle and number of cycles are the output of this program. A sample calculation is shown in Appendix C.

The sensitivity of this program to errors in crack length measurement was investigated to define the required measurement accuracy. Figure 3-3 shows a plot of this error. For example, when both coupon crack lengths entered into the program were 0.020 in. greater than the correct lengths, the program calculated a stress value of 0.5 percent less than correct value and the number of cycles 2.8 percent greater than the actual number.

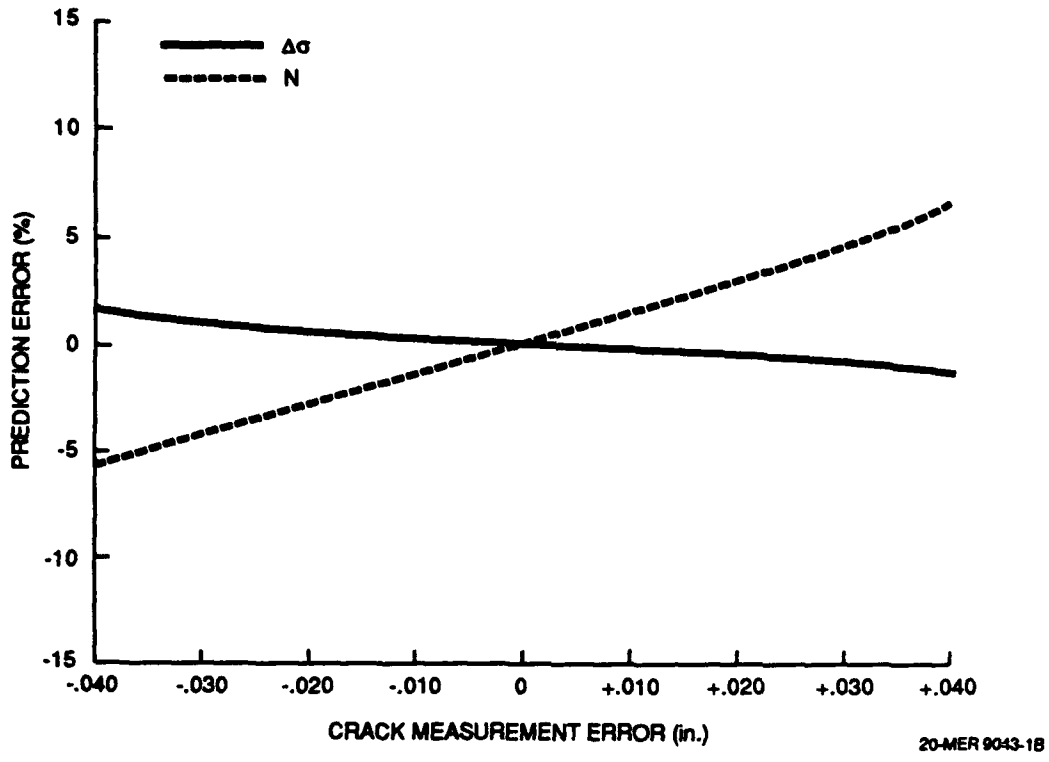

Figure 3-3. Stress Histogram Prediction Error versus Crack Measurement Error

3.4 Computer Program for Fatigue Life

A general computer program can be written for the evaluation of fatigue damage at all the critical locations of the bridge using the Miner law. As shown earlier, only one twin coupon system is required, which can be located at any convenient location, to determine the histogram. For a given bridge, the number of stress cycles for all the locations will be the same, whereas the stress levels will be proportional to the stress value indicated by the coupon system at its location. The constants of proportionality can be determined through a Finite Element analysis, or experimentally, using strain gauges, through crossing tests. Thus knowing $\Delta\sigma_i$ and N for each critical location, Equation 3-10 can be applied to determine the fatigue damage. Identification of the critical locations, and development of the computer program for fatigue life consumed at these locations will be one of the tasks in the subsequent phase of the work.

4. COUPON DESIGN

Two coupons of identical geometry, but made from different materials, were designed. The goal was to select materials, and optimize width, thickness, and initial crack length so that significant crack growth occurs under fatigue loading. For this design, the Paris crack growth law (Eq. 3-1,3-2) was used as the theoretical model for crack growth.

4.1 Bridge Selection

The Armored Vehicle Launched Bridge (AVLB) shown in Figures 4-1 and 4-2 was identified as the candidate bridge for field testing of the fatigue life indicator concept.

This selection was made for the following reasons:

- Since the AVLB is currently in service, the development of the fatigue life indicator will provide immediate assistance to the Army

- Crossing tests are being performed in Fall '90 on the AVLB at Aberdeen Proving Grounds. This provides an excellent opportunity for field validation of the FLI system

- The AVLB is a mechanically launched bridge and thus more cost-effective for field validation testing than the labor intensive manually launched bridges

- The FLI technology developed for the AVLB can easily be extended to yield a universal FLI design. This would be applicable to both manually launched (MGB) and mechanically launched (LAB, HAB, Leguan, Dornier Folding Bridge) military bridges currently in service/evaluation/development.

The AVLB is a scissors launched bridge capable of being launched both be the M48 and the M60 launch vehicles. The bridge superstructure has two treadways interconnected by cross bracings. Each of the treadways is of tapered construction comprised of two identical girders connected through a structural hinge. Each girder is of rivetted plate/girder construction.

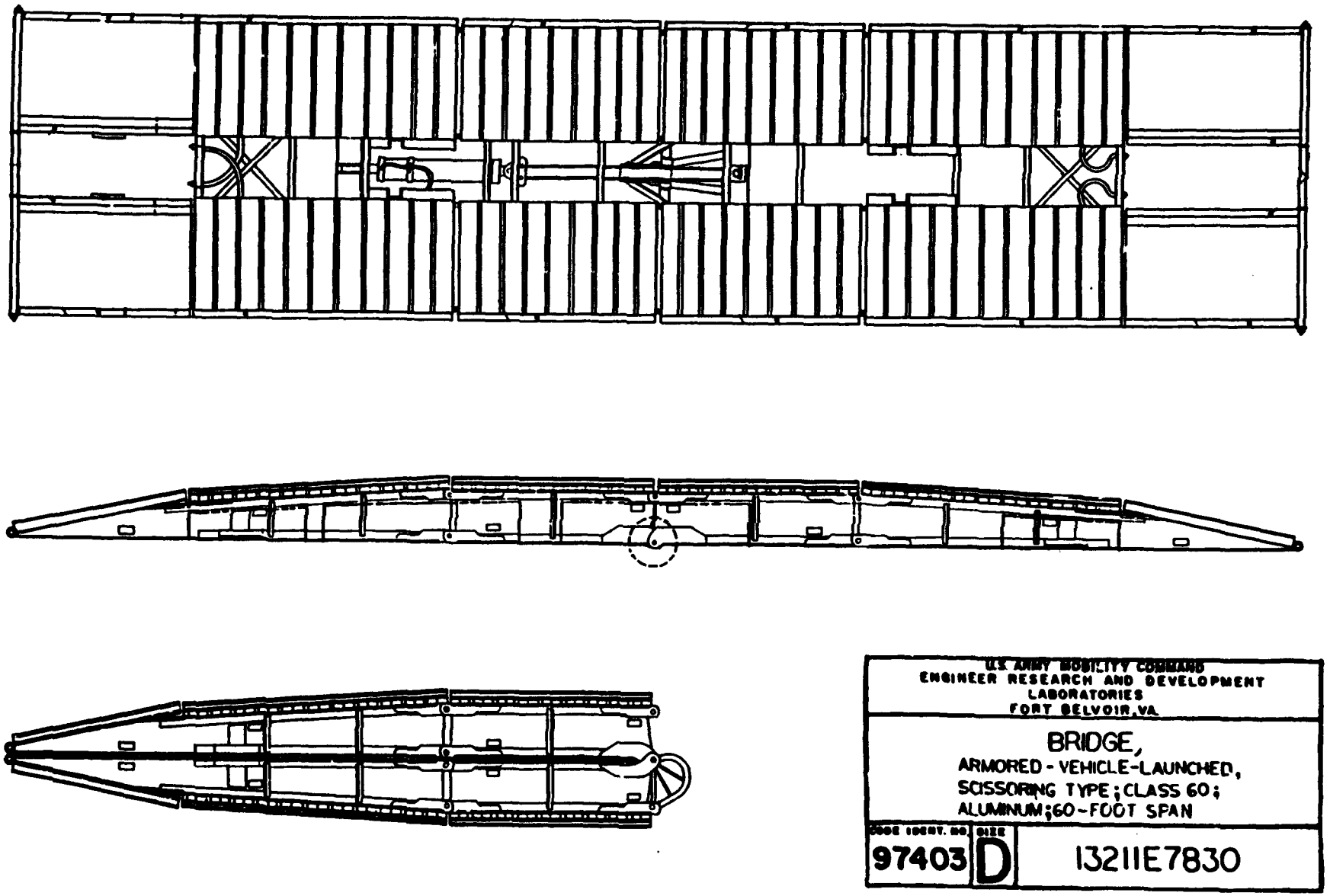

Figure 4-1. Armored Vehicle Launched Bridge (AVLB)

Figure 4-2. Armored Vehicle Launched Bridge (AVLB)

The deck is comprised of a number of extrusions that span transverse to the bridge length. These extrusions are bolted to the top flange of the tapered plate girder. Tapered vertical plates, forming the girder webs, are rivetted to the bottom and top flanges to form the plate girder. The webs of each girder are connected by a number of diaphragms to provide cross-sectional rigidity.

When a vehicle traverses the bridge, its load is transferred from the deck to the plate girder and finally to the banks. The mechanisms of load transfer in the treadway are through flexural bearing, direct shear and torsional shear stresses. The predominant load transfer at the treadway center is by flexure and at the ends by shear. The flexure causes tensile stresses in the treadway's bottom chord.

From test data provided by the Directorate of Combat Engineering at Ft. Belvoir, VA, a 60-ton vehicle results in a stress cycle of 16.5 Ksi in the bottom tension chord near the bridge center span. The bridge has a defined life of 10,000 crossings of this magnitude.

4.2 Material Selection

Several materials were considered for the coupon design. Published crack propagation constants (2), shown in Table 4-1 were used to identify two materials which would exhibit acceptable crack growth.

Preliminary calculations were made and the fatigue crack growth data generated for these materials are shown in Table 4-2. From these data, 2024-T3 Aluminum and 6061-T6 Aluminum were chosen as the candidate coupon materials because their final crack length was approximately 1.5 in. 7075-T6 Aluminum was initially selected but replaced by 6061-T6 because of material availability problems. 6061-T6 is an adequate replacement for 7075-T6 as laboratory testing yielded good results.

Final coupon design was done using a width of 4 in. This was selected to allow the crack to grow to the useful width of the coupon in 10,000 cycles. Final calculations of fatigue crack growth rates yielded the plot shown in Figure 4-3 for the two selected materials.

Table 4-1. Paris Crack Growth Constants

Material	C (in/cycle)	n
Aluminum 2024-T3	1.278×10^{-9}	3.32
Aluminum 7075-T6	1.413×10^{-8}	2.73
Aluminum 6061-T6	1.55×10^{-8}	2.73
Steel (Martensitic)	66×10^{-8}	2.25
Titanium alloy Ti-7Al-2Cb-1Ta	6.4×10^{-13}	5

Table 4-2. Fatigue Crack Growth Data
Δs = 24 Ksi

No. of Cycles N	7075-T6 a_i=0.1 in.	6061-T6 a_i=0.1 in.	2024-T3 a_i=0.2 in.	Steel a_i=0.25 in.	Titanium a_i=0.5 in.
1,000	0.120	0.116	0.225	0.257	0.516
2,000	0.146	0.150	0.255	0.263	0.534
3,000	0.170	0.189	0.293	0.27	0.554
4,000	0.255	0.240	0.342	0.277	0.575
5,000	0.288	0.316	0.405	0.285	0.598
6,000	0.378	0.426	0.491	0.292	0.625
7,000	0.512	0.594	0.611	0.3	0.654
8,000	0.720	0.872	0.790	0.308	0.686
9,000	1.064	1.361	1.077	0.316	0.724
10,000	1.680	2.011	1.588	0.324	0.766

The final coupon design is shown in Figure 4-4.

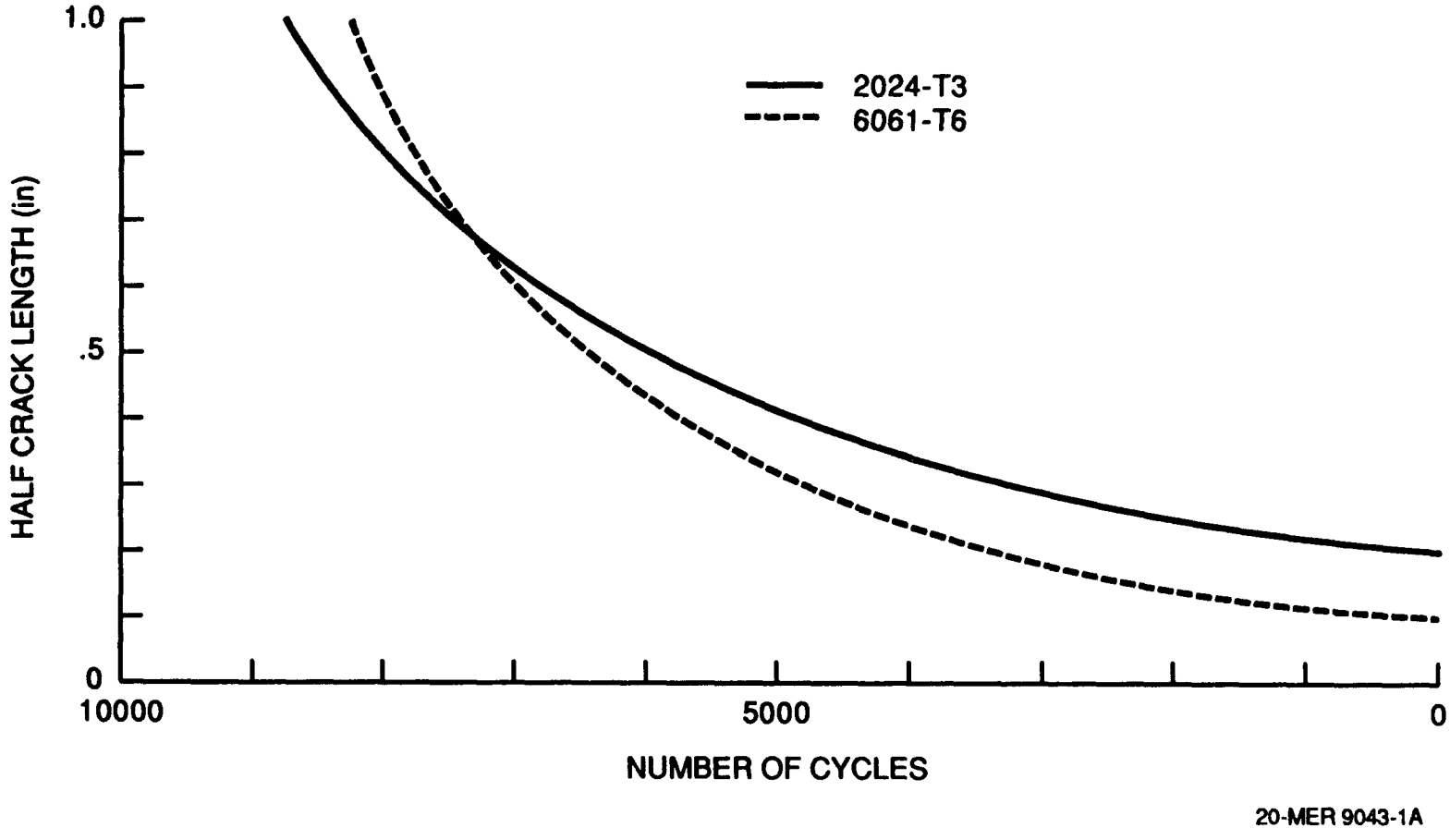

Figure 4-3. Calculated Crack Growth in 4.0 in. Wide Coupons

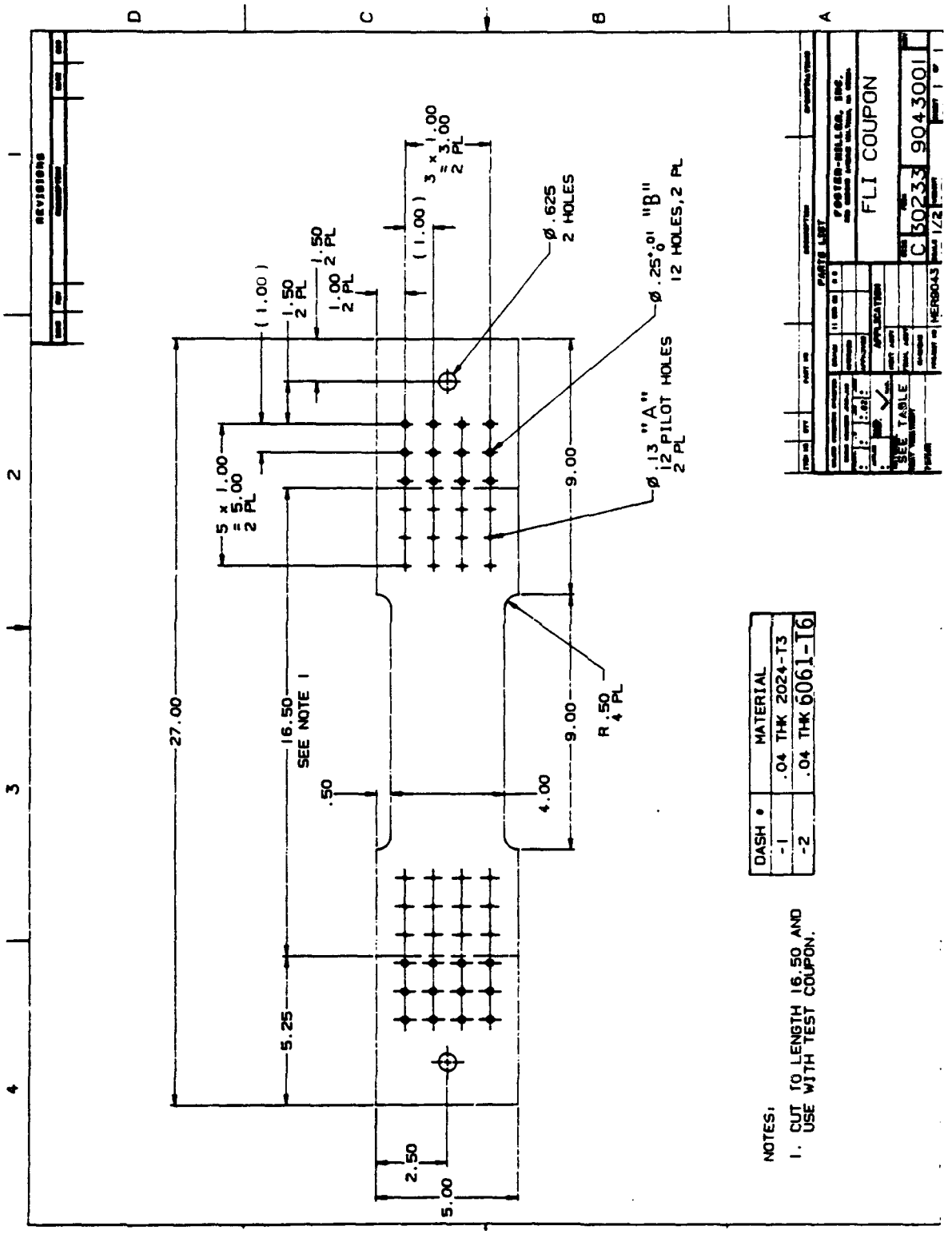

Figure 4-4. Fatigue Life Indicator Coupon Design

4.3 Coupon Manufacturing

For lab testing, all FLI coupons were manufactured from the same sheet stocks of 2024-T3 and 6061-T6, respectively. Future FLI coupons will demonstrate nearly identical crack growth characteristics as the defined composition and heat treatments of these alloys constrain their crack growth properties to a narrow scatter.

FLI coupons are cut with the grain direction of the material longitudinal to the coupon. This is done to prevent inconsistencies which would arise from any strength difference between the two directions.

Each coupon is fatigue cycled individually to introduce its required initial crack length. A 0.040 diam hole, which is sufficient to permit passage of a 5 mil. jeweler's saw blade, is drilled in the center of the coupon. The short jeweler's saw cut of approximately half of the required initial crack length is then made in each side of the hole. Steel doubler plates are then bolted to the coupon using the holes market "B" in Figure 4-4. This assembly is cycled at 2 Hz until cracks are observed to grow to their required initial lengths. The stress level for cycling was determined to be significant by later testing. This level should always be less than the expected working stress of the applicable bridge at the expected attachment location. The required initial crack length is also defined for the expected application. It is desirable to have the cracks grow to the full useful width of the coupon during the expected life of the system. The greater the crack growth, the less error due to measurement system resolution. Thus, using the expected stress levels and the Paris Crack Law (Eq. 3-1), initial crack lengths are selected which will cause the cracks to grow to the full useful width of the coupons during the expected life of the system. Figure 4-5 is a magnified photo of 6061-T6 coupon after pre-cracking.

After the required initial crack length is present, the steel doubler plates are removed and the coupon is cut to its final length of 16.5 in. This process of removing the coupon area used for loading during pre-cracking was included to remove any coupon damage which may have occurred during pre-cracking.

4.4 Coupon Attachment

The success of this concept depends on the strain in the parent structure being transferred to the FLI coupons. Several methods were considered for use in this rigid attachment. These methods were compared on both their effectiveness in creating a rigid attachment and their relative ease of application.

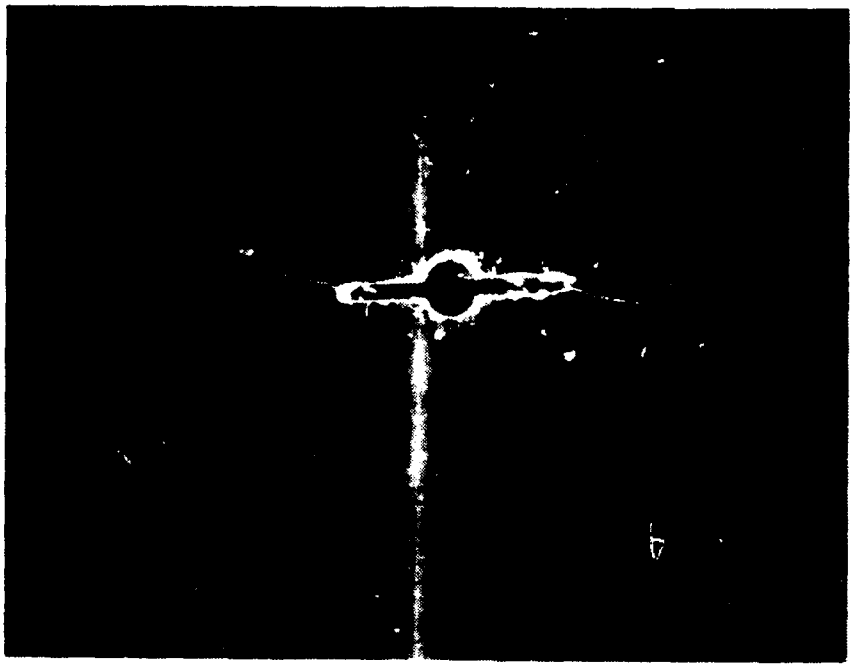

Figure 4-5. Pre-cracked 6061-T6 FLI Coupon

Bonding

The review of literature on other, similar methods of coupon crack growth indicated that bonding was the preferred attachment method. Bonding will provide excellent strain transfer when the bonding agent is properly selected and used. However, this method has some disadvantages. Bonding requires a skilled technician and timely surface preparation. Long-term exposure risks bond degradation or failure. Additional research will be required to resolve the key issues related to the bonding method. Mechanical methods using bolts have been used in the work performed here primarily to demonstrate the twin coupon concept.

Huck Bolts - Coupon Assembly A

The first attachment method tested was the use of "Huck" bolts. These are blind fasteners which expand to hole size and provide clamping force. Figure 4-6 shows photos of both sides of coupon assembly A. The 2024-T3 FLI coupon was attached flat against the test coupon on the hulk bolt head side. The 6061-T6 FLI coupon was deformed by the expanding fasteners on the other side. This deformation left a center bulge of 0.04 in. between the FLI coupon and the test coupon. This assembly was statically tested to an axial load of 34 Kips with the recorded strains shown in Figure 4-7. As shown in this figure, the test coupon demonstrated linear strain with

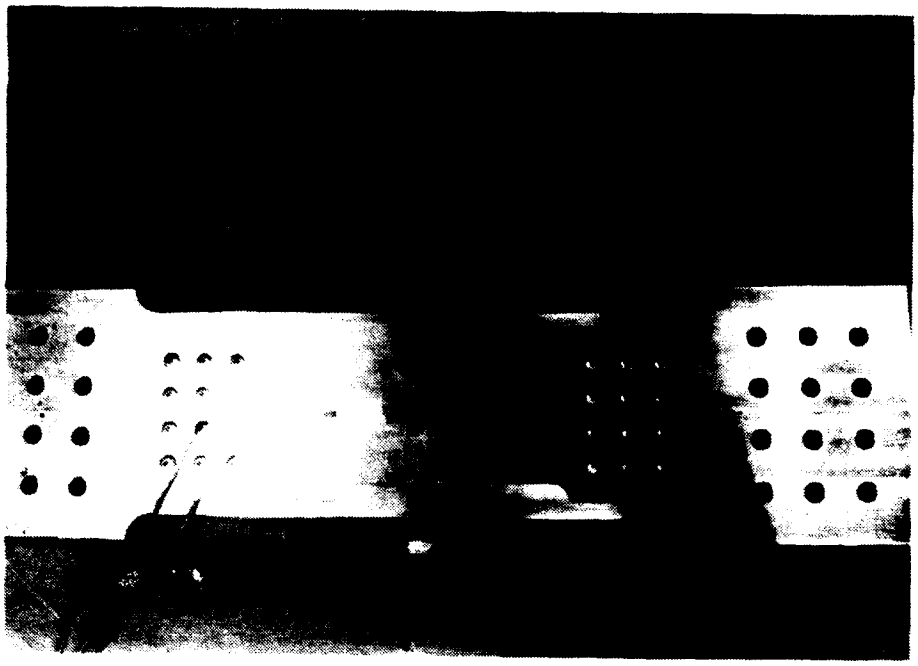

2024-T3 SIDE

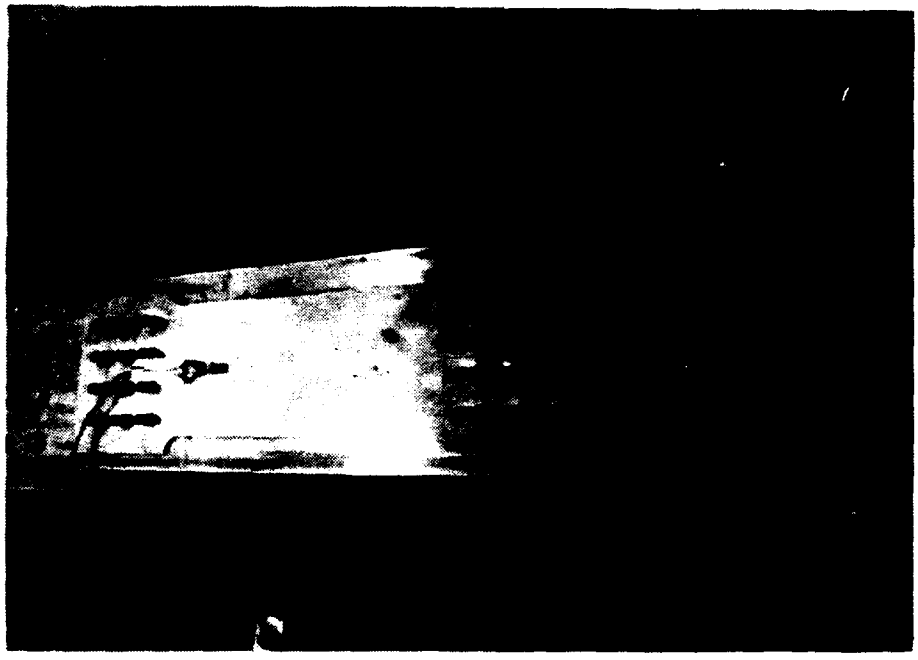

6061-T6 SIDE

Figure 4-6. Coupon Assembly "A"

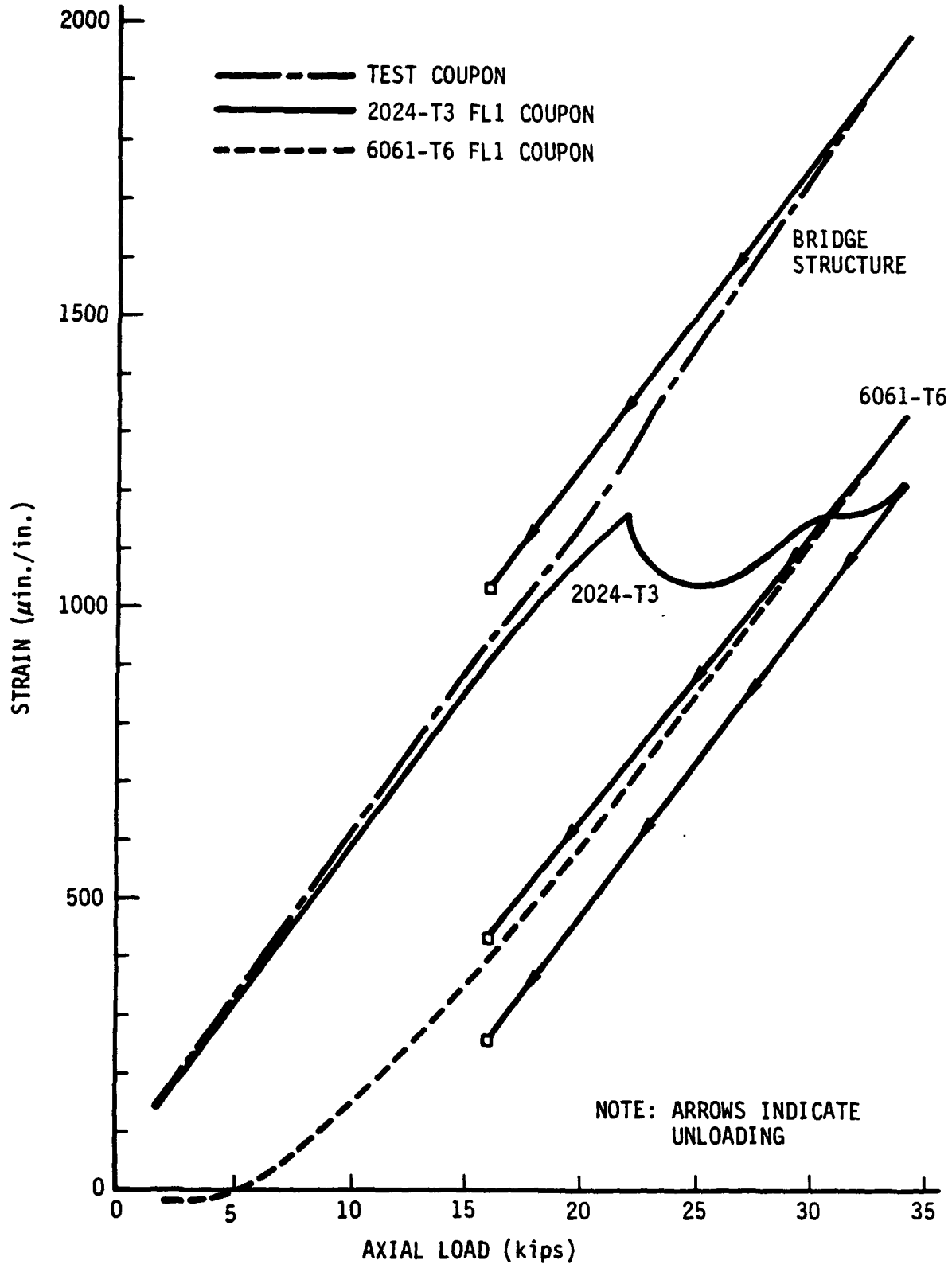

Figure 4-7. FLI Coupon Assembly "A"

load. The 2024-T3 FLI coupon demonstrated better than 90 percent strain transfer up to a stress of approximately 12 Ksi. Further increases in load demonstrated this to be the maximum stress which could be sustained by this coupon.

The 6061-T6 FLI coupon demonstrated little strain up to a test coupon elongation of 300 to 400μ in./in. which brought the 6061-T6 coupon flat against the test coupon. This FLI coupon then demonstrated better than 80 percent strain transfer up to a stress of approximately 14 Ksi where the test was halted.

Post-test inspection at zero load revealed that the 6061-T6 FLI coupon had returned to its pre-test bulged position. However, the 2024-T3 FLI coupon now had a center bulge of 0.06 in. away from the test coupon. Post-disassembly inspection revealed no visible damage to the 6061-T6 FLI coupon. The 2024-T3 FLI coupon appeared to have some attachment hole deformation. This deformation, coupled with any tolerance gaps that existed on assembly would account for the observed slippage under load. Friction from the Huck bolt clamp-up force would be sufficient to prevent the coupon's return to its original position. Thus, the FLI coupon bulged out as the test coupon returned to its unstrained length.

As a result of this test, the Huck bolt attachment method was considered unacceptable and was not further considered.

Standard Bolts - Coupon Attachment Test 1

The results of the testing of coupon assembly "A" indicated that the FLI coupon attachment method had to be optimized before crack growth testing could proceed. For this optimization test, one smaller, uncracked coupon was used to demonstrate the attachment method.

A configuration consisting of 6-1/4 in. bolts and a steel doubler plate was used for each end of the coupon. A drawing and a photo of the assembly are shown in Figures 4-8 and 4-9, respectively. The bolts were torqued to 120 in./lb which gives a tension load of approximately 2,500 lb per bolt. The 1/8-in. thick steel plates distribute this load to make a friction joint instead of the bearing joint of coupon assembly "A." This assembly was statistically tested to an axial load of 38 Kips with the recorded strains shown in Figure 4-10. As shown in this plot, strain transfer was excellent with less than a 2 percent difference between the two recorded strains.

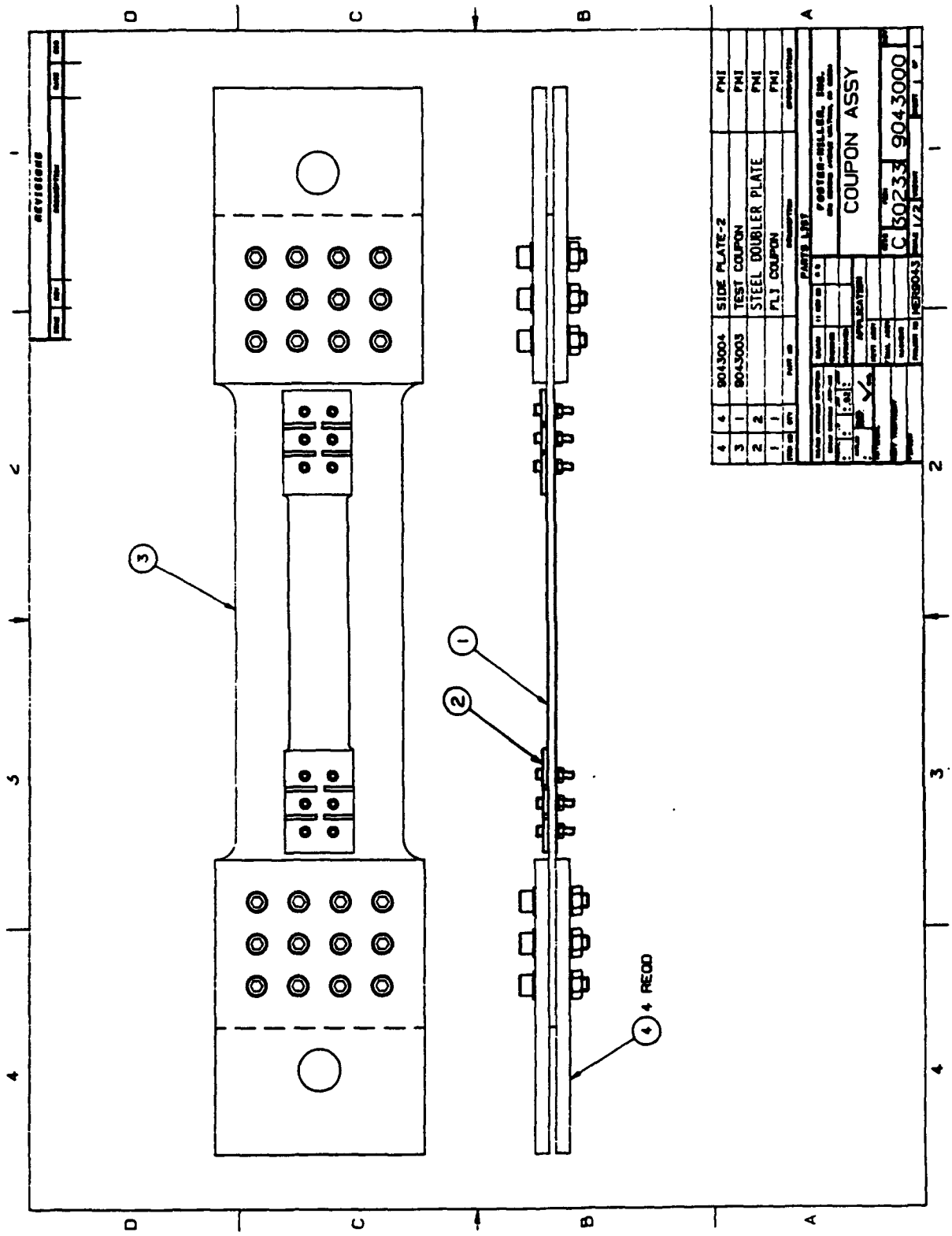

Figure 4-8. Coupon Attachment Test No. 1

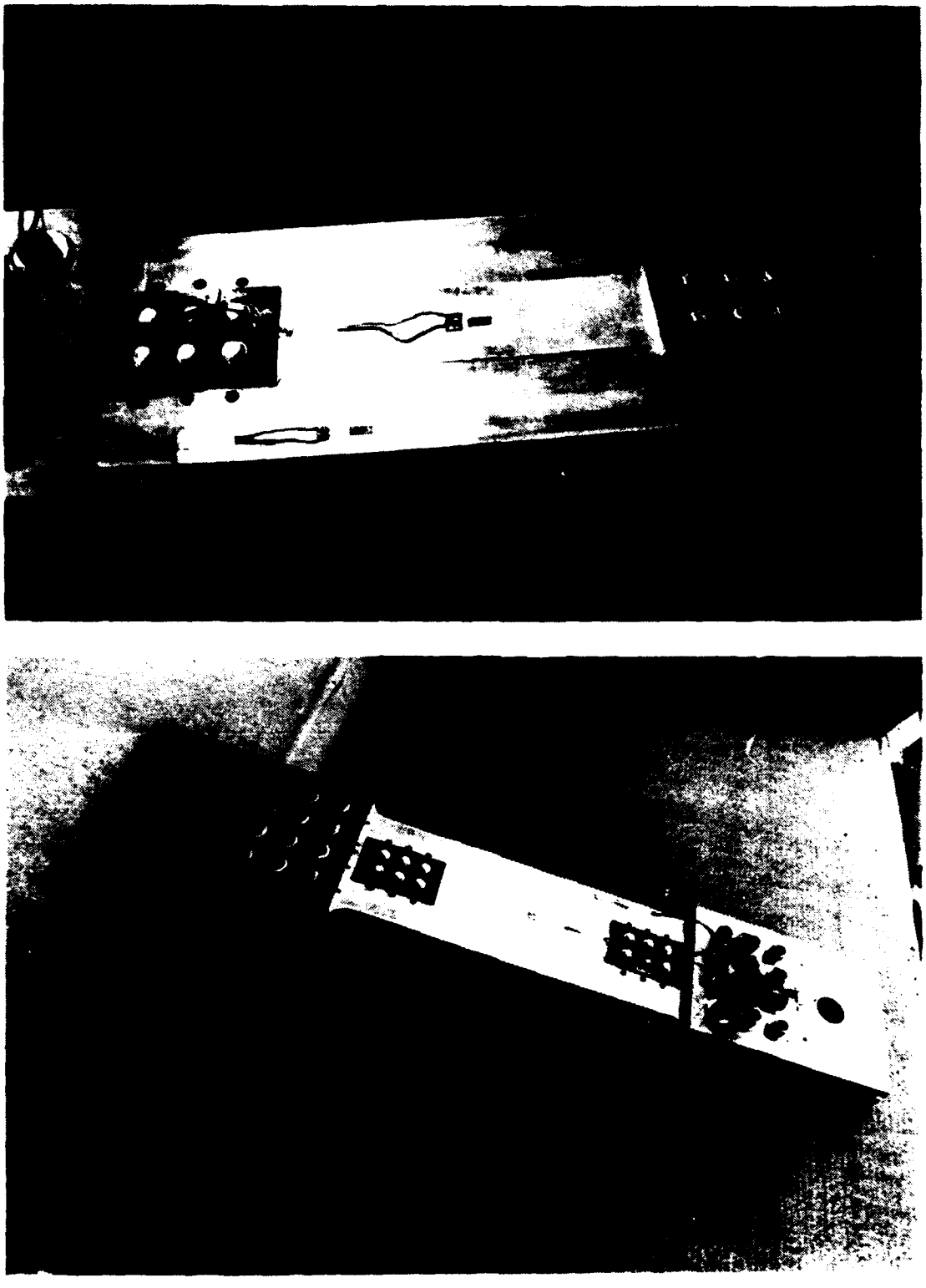

Figure 4-9. Coupon Attachment Test No. 1

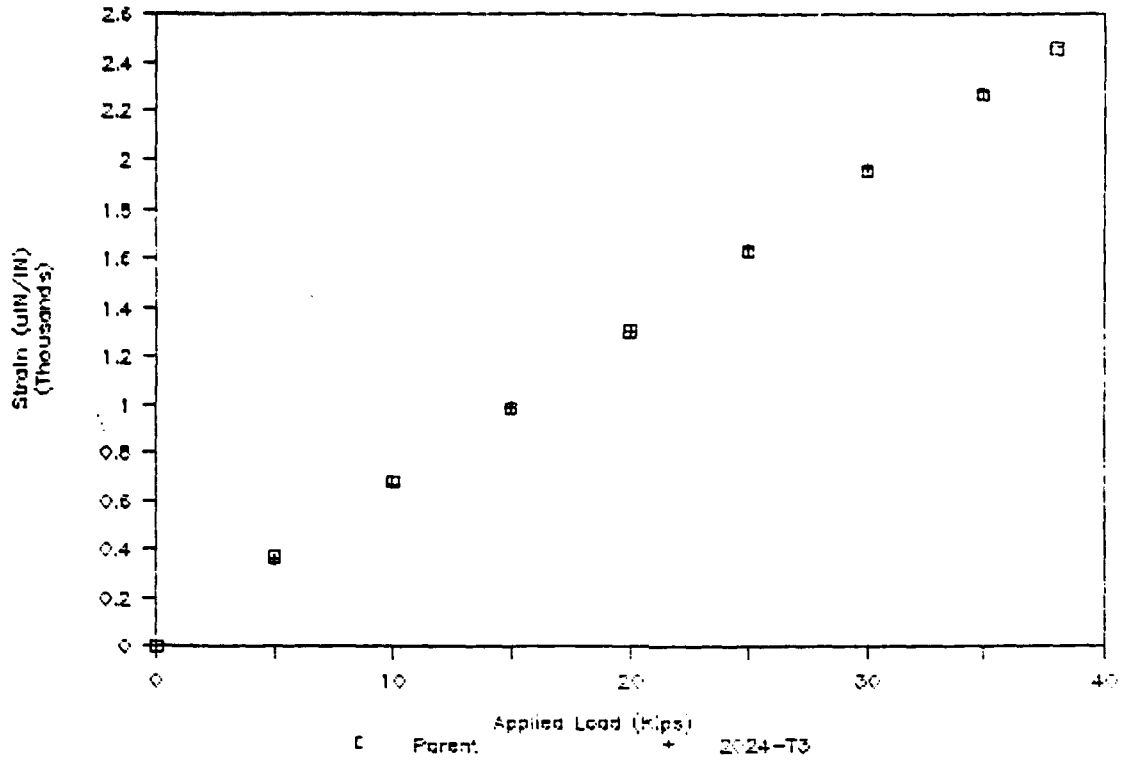

Figure 4-10. Attachment Test No. 1
(Static Test Before Cycling)

This assembly was loaded dynamically from 3.8 to 38 Kips for 10,000 cycles. Static loading after 5,000 and 10,000 cycles indicates no loss in strain transfer. As shown in Figure 4-11 there was less than a 4 percent difference between the two recorded strains after 10,000 cycles.

As a result of this test, the standard bolts with doubler plate attachment method was considered acceptable. The remaining laboratory tests confirmed this to be an acceptable attachment method. However, in the later laboratory tests, the doubler plates were changed from 1/8 in. steel to 1/4 in. 7075-T6 Aluminum to avoid any corrosion problems when this system is used in the field. A drawing of the final test configuration is shown in Figure 4-12. A drawing of the doubler plate is shown in Figure 4-13. The attachment procedure is described in Appendix D.

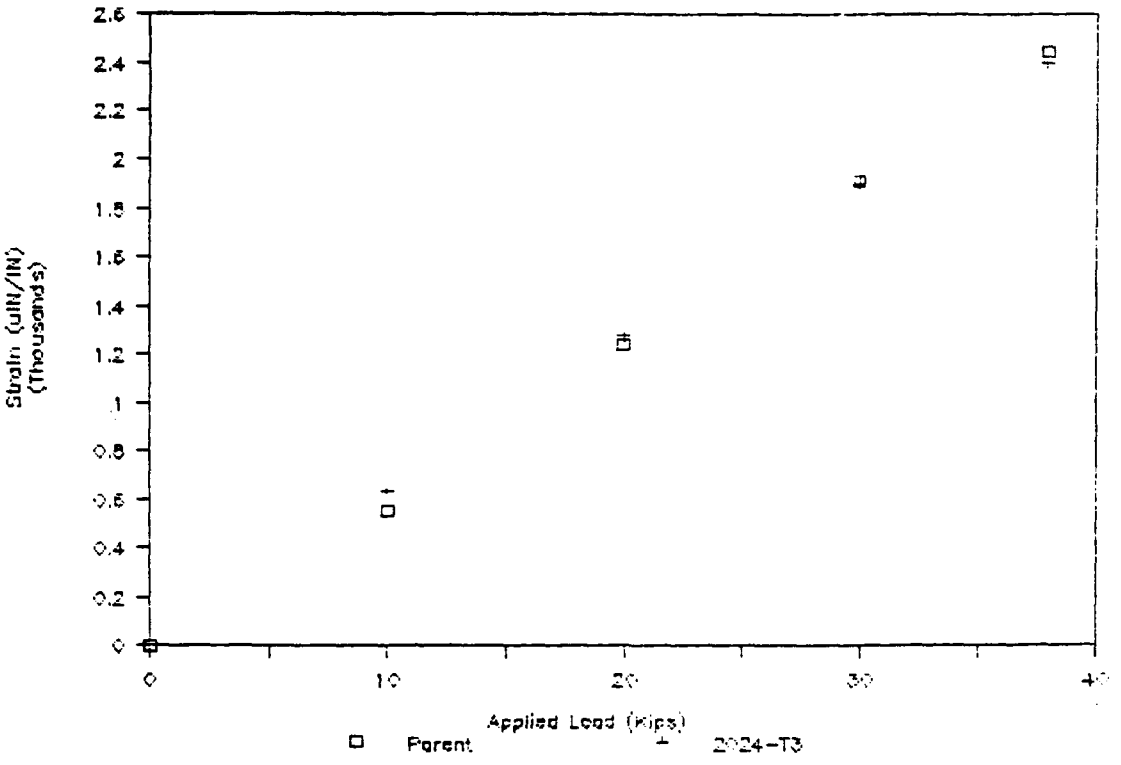

Figure 4-11. Attachment Test No. 1
(Static Test After 10,000 Cycles)

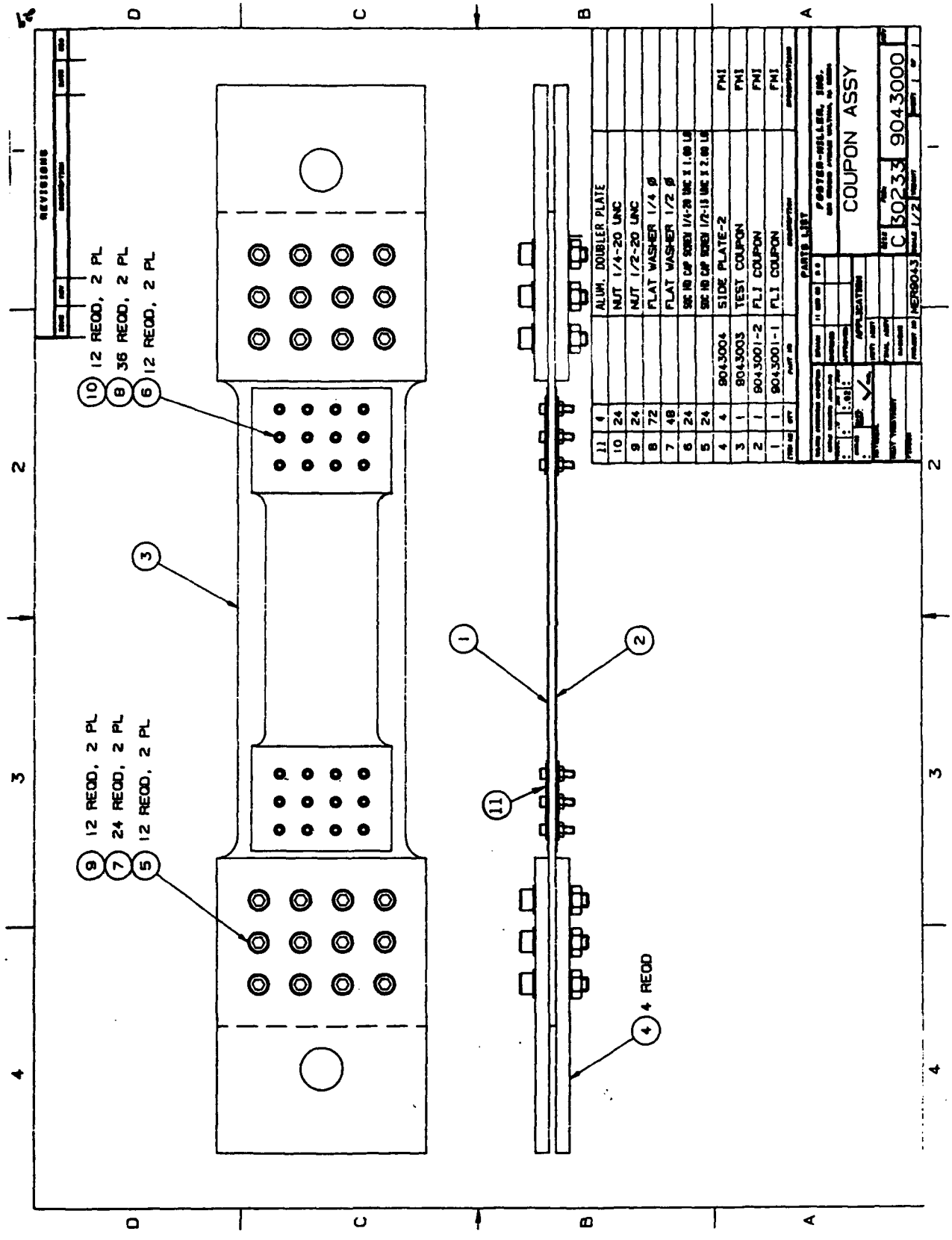

Figure 4-12. Final Test Configuration

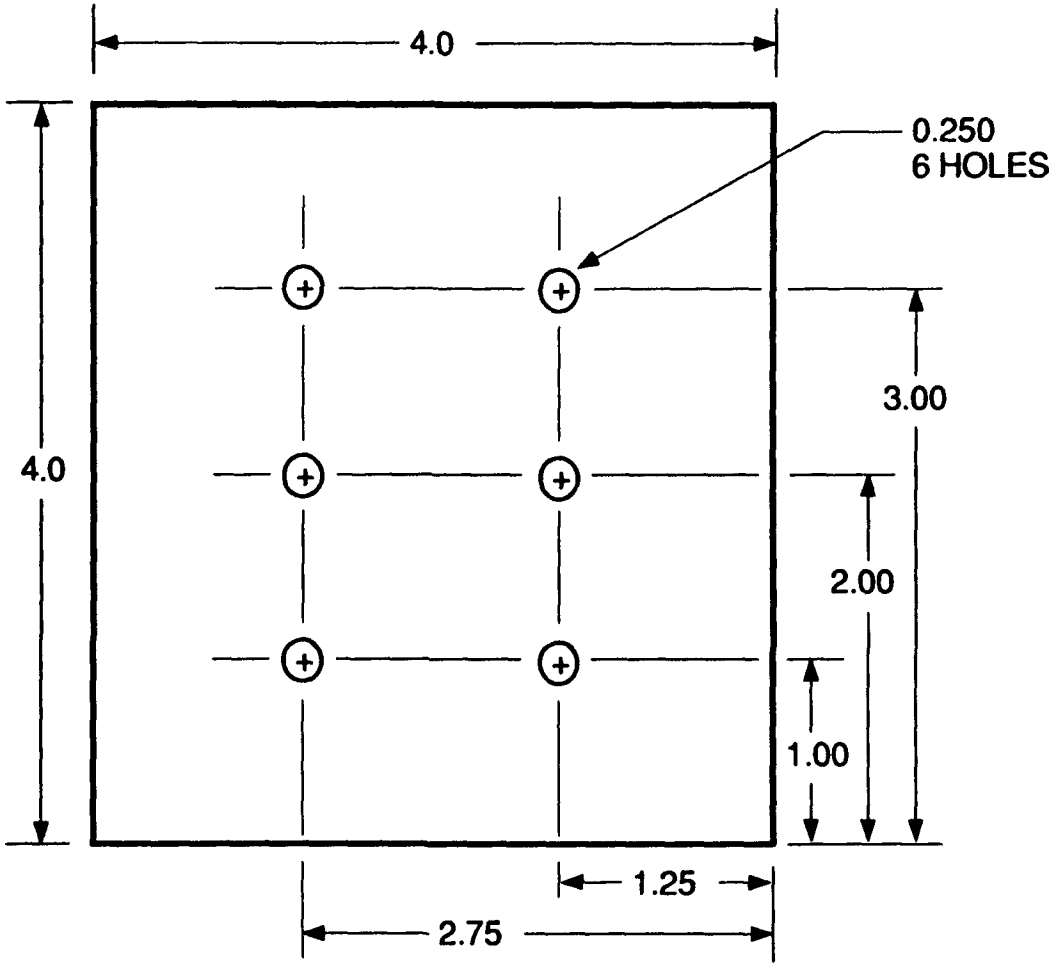

NOTES:

1. MATERIAL: SHEET, .250 THICK
   6061-T6 ALUMINUM

20-MER 9043-3

Figure 4-13. Doubler Plate

5. LABORATORY TESTING

A total of 11 full FLI assembly tests were performed to prove this concept. These tests validated the coupon attachment method, defined the Paris Crack Law constants, and verified the ability of the computer program to correctly determine the loading histograms.

5.1 Test Facility

The two FLI coupons were mounted on opposite sides of a representative bridge parent coupon. This arrangement was used to save space in the test facility. In actual practice, the two coupons are likely to be mounted end to end or side by side. This assembly, shown in Figure 5-1, was mounted in an Instron 8502 tensile test machine with single pin connections at each end. Steel side plates transferred the load from the machine to the parent coupon. This facility is shown in Figure 5-2.

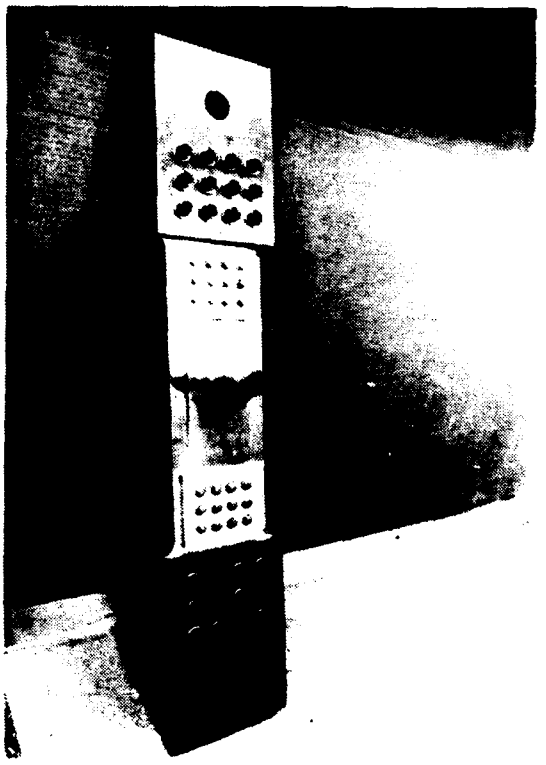

Figure 5-1. FLI Test Assembly

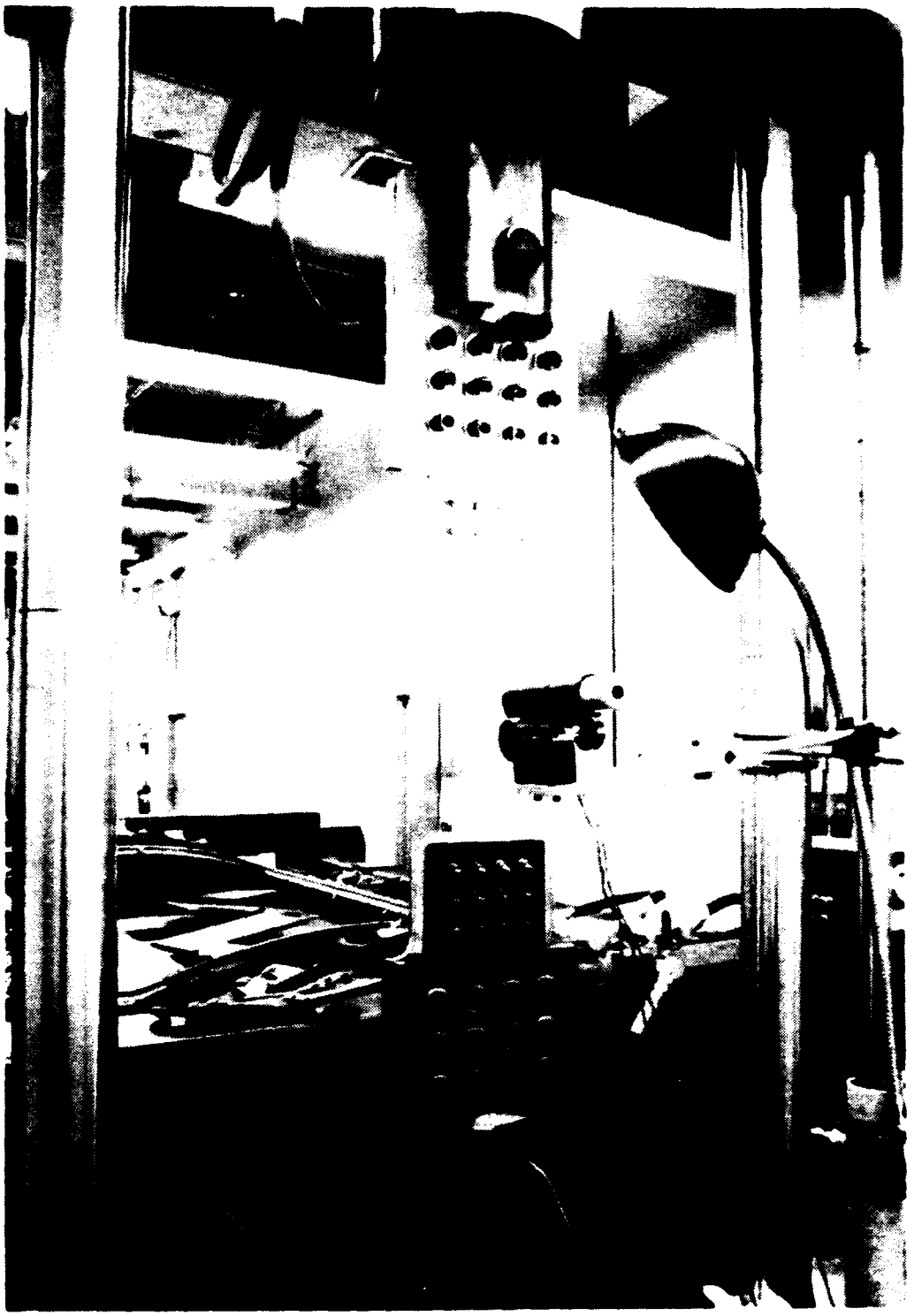

Figure 5-2. FLI Test Facility

The Instron machine controlled the loading of the assembly. Static loading was done in step intervals to the maximum stress that would occur in the dynamic test. This was done to check the coupon attachment for slippage. Dynamic loading was done in a sine wave at a frequency of 2 Hz and a loading ratio of less than 0.10.

5.2 Instrumentation

The FLI coupons and parent coupon were strain gauged for the attachment method tests. These gauges and the applied load were recorded using an ACRO900 data acquisition system. For later tests, load was only monitored directly on the Instron machine. FLI coupon cracks were measured with a graduated microscope. These crack lengths were measured to an accuracy of 0.002 in. As shown in Figure 3-3, this results in negligible stress histogram prediction error due to measurement error.

5.3 Strain Transfer

The transfer of strain from the parent structure to the FLI coupons was measured to quantify the effectiveness of the attachment method. Strain gauges were mounted on both FLI coupons and the parent coupon of the finalized configuration. This assembly was loaded to 42.7 Kips (24 Ksi) with excellent strain transfer as shown in Figure 5-3.

5.4 Test Matrix

A summary of the tests performed is given in Table 5-1. Assemblies A, B and C were preliminary configuration tests which defined the coupon attachment method and the initial crack lengths for later testing. Two full assembly tests were then performed at a stress range of 24 Ksi, to define the Paris Crack Growth Law constants for both of the coupon materials. The failure of the 0.25 in thick 7075-T6 aluminum parent coupon in Assemblies D and F, as shown in Figure 5-4, required two additional tests (E and G) to be performed. With the crack law constants defined, four proof-of-concept tests were performed. Assemblies H and I were tested at 20 Ksi and then at 25 Ksi to check if this load histogram could be reconstructed from the crack length measurements. Concern over crack retardation due to pre-cracking at 24 Ksi led to two additional tests. Assembly J, tested at the expected AVLB stress range of 17 Ksi, was pre-cracked at 15 Ksi. Assembly K, also pre-cracked at 15 Ksi, then repeated the tests of Assemblies H and I to define the retardation effects.

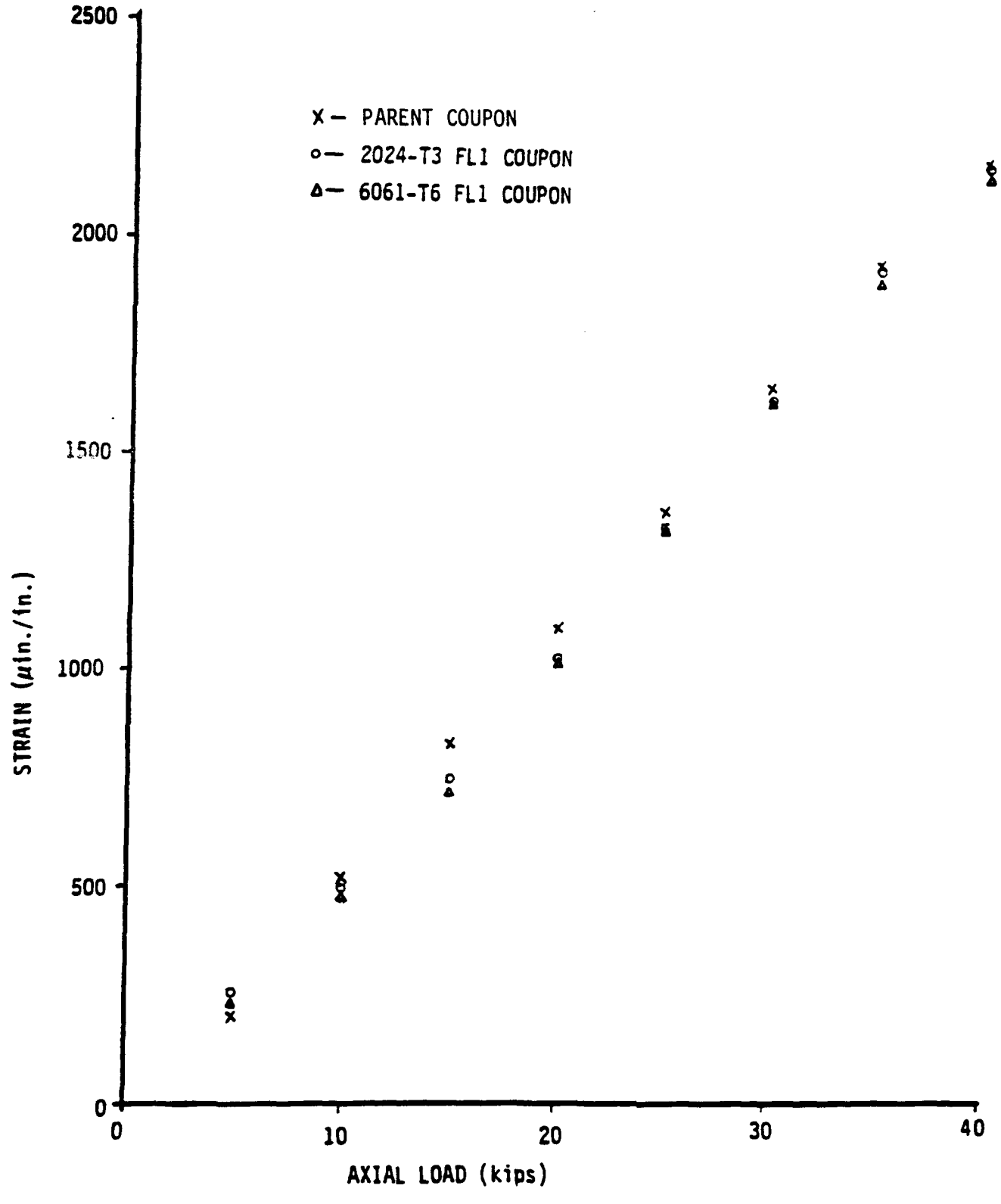

Figure 5-3. Strain Transfer in Assembly

Test Series*	Assembly	Attachment Method	Fatigue Stress Range (Ksi)	Initial Crack Length 2024-T3 (in.)	Initial Crack Length 6061-T6 (in.)	Pre-cracking Stress Range (Ksi)	Comments
I	A	Huck bolts -	-	-	-		Attachments yielded in static test
	B	Bolts with steel doubler plates	22	0.20	0.10	24	Full assembly using bolted attachment with steel doubler plates
	C	Bolts with steel doubler plates	22	0.13	0.10	24	Adjustment of initial crack length
II	D	Bolts with steel doubler plates	24	0.15	0.10	24	Parent coupon failed
	E	Bolts with steel doubler plates	24	0.15	0.10	24	Basis for determination of Paris Crack Law constants
	F	Bolts with steel doubler plates	24	0.15	0.10	24	Parent coupon failed
	G	Bolts with steel doubler plates	24	0.15	0.10	24	Verification of Paris Crack Law constants
III	H	Bolts with steel doubler plates	20-25	0.20	0.13	24	Multiple stress range test
	I	Bolts with steel doubler plates	20-25	0.23	0.13	24	Verification of multiple stress range test
	J	Bolts with aluminum doubler plates	17	0.20	0.20	15	Low stress pre-cracking, AVLB stress range, aluminum doubler plates
	K	Bolts with aluminum doubler plates	20-25	0.20	0.20	15	Multiple stress range test with low stress pre-cracking

* I - Preliminary Configuration Tests
II - Paris Law Constants Evaluation Tests
III - Proof-of-Concept Tests

Table 5-1. Fatigue Life Indicator Test Matrix

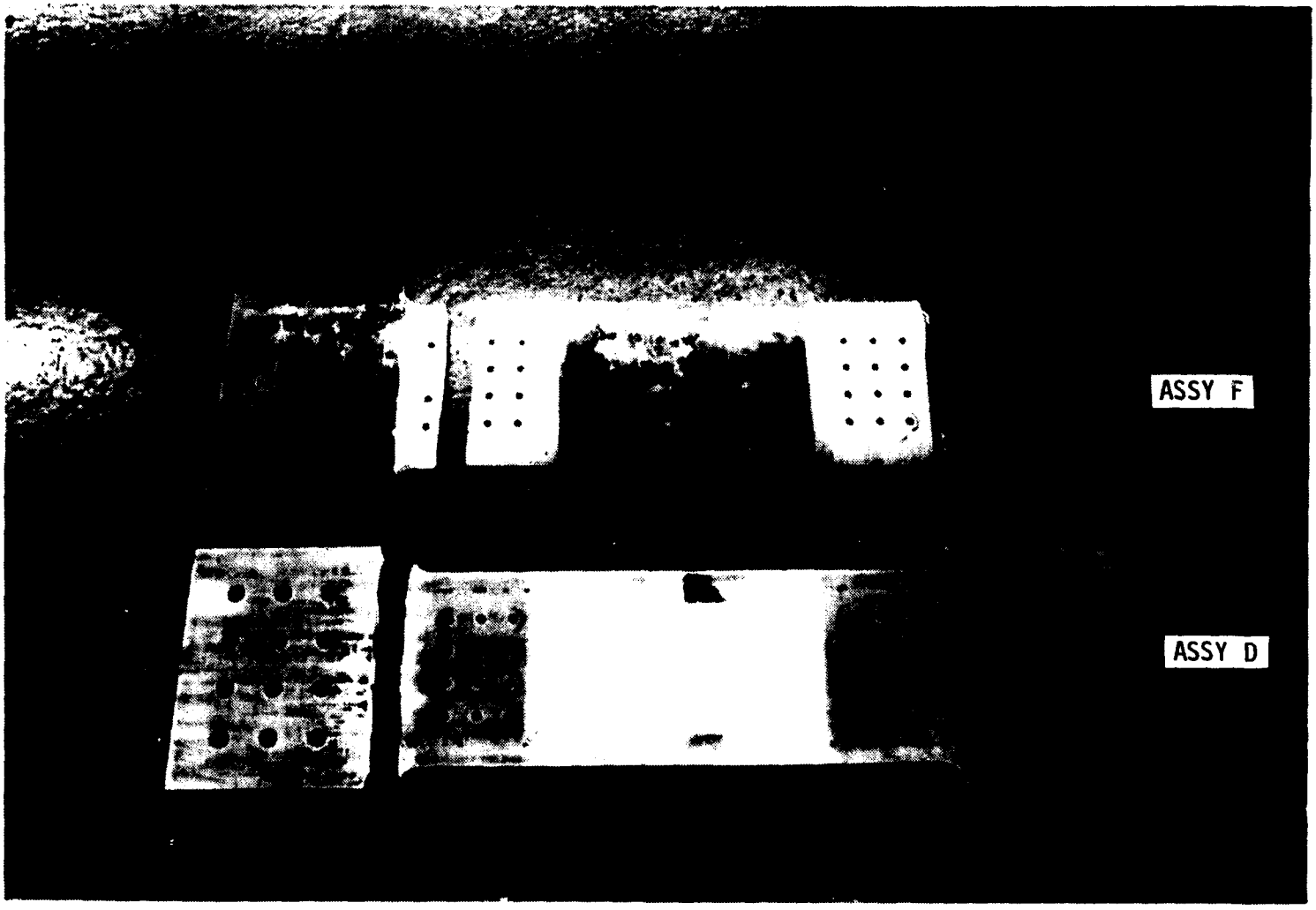

Figure 5-4. Failed Parent Coupons

6. TEST RESULTS

6.1 Preliminary Configuration Tests

Assemblies A, B, and C defined the coupon attachment method and finalized the test procedure. The bolted attachment with doubler plates demonstrated excellent strain transfer. The adjustment of the initial crack lengths provided preliminary definition of the crack growth rates by causing significant crack growth to occur in both coupons during testing.

6.2 Paris Law Constants Evaluation Tests

The Paris Crack Law constants for the two coupon materials were defined from the results of assemblies E and G. Preliminary definition of these constants was made using a least squares fit to the logarithm of the da/dN and dK test data. A linear fit was found to give good results for the 2024-T3 coupon. However, the 6061-T6 coupon required a bi-linear fit to achieve good correlation. This is most likely due to the much lower fracture toughness of the 6061-T6 coupon. This bi-linear fit of the data is also evident in the published data (2) shown in Figure 6-1. A linear fit of the 6061-T6 data would have resulted in increased error in the stress histogram calculations.

The preliminary constants were then adjusted to account for averaging over the data intervals and any errors in a particular measurement. The final constants defined by the testing are given in Table 6-1. Figures 6-2 and 6-3 show all of the test data for the 2024-T3 and 6061-T6 coupons with the fit lines of their respective constants. The point where the two lines of the bi-linear 6061-T6 fit intersect is defined in this report as the transition point. With the Paris Crack Law constants defined, the initial coupon crack length could be chosen for subsequent tests as described in subsection 4.3.

Table 6-1. FLI Paris Crack Law Constants

Material	da/dN	Test C (μin./cycle)	Test n	Published (2) C (μin./cycle)	Published (2) n
2024-T3	All	2.4E-4	4.015	1.3E-3	3.32
6061-T6	<Tr	4.9E-2	2.17	1.6E-2	2.73
	>Tr	9.0E-6	4.90	1.6E-5	4.80

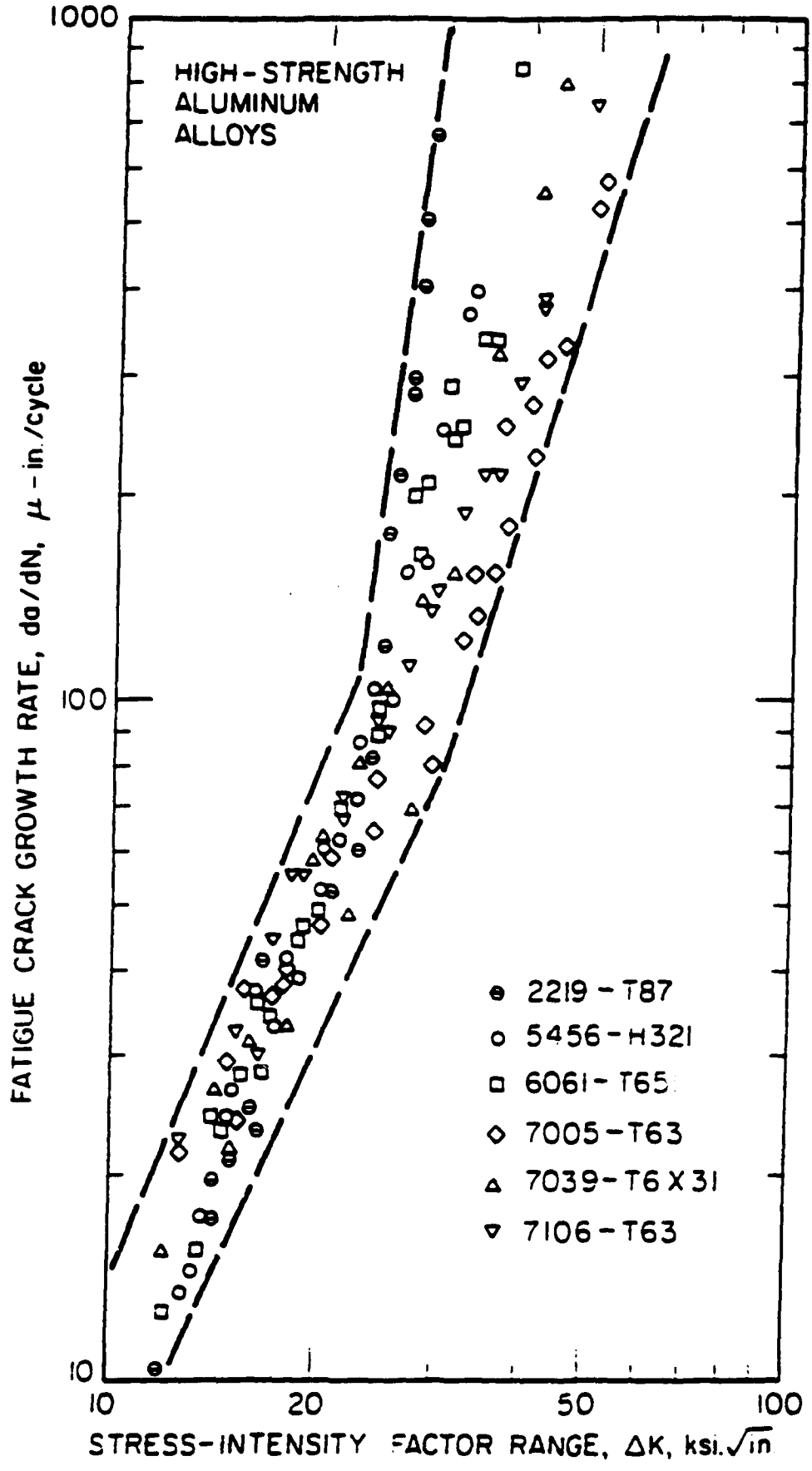

Figure 6-1. Crack Growth Data for High Strength Aluminum

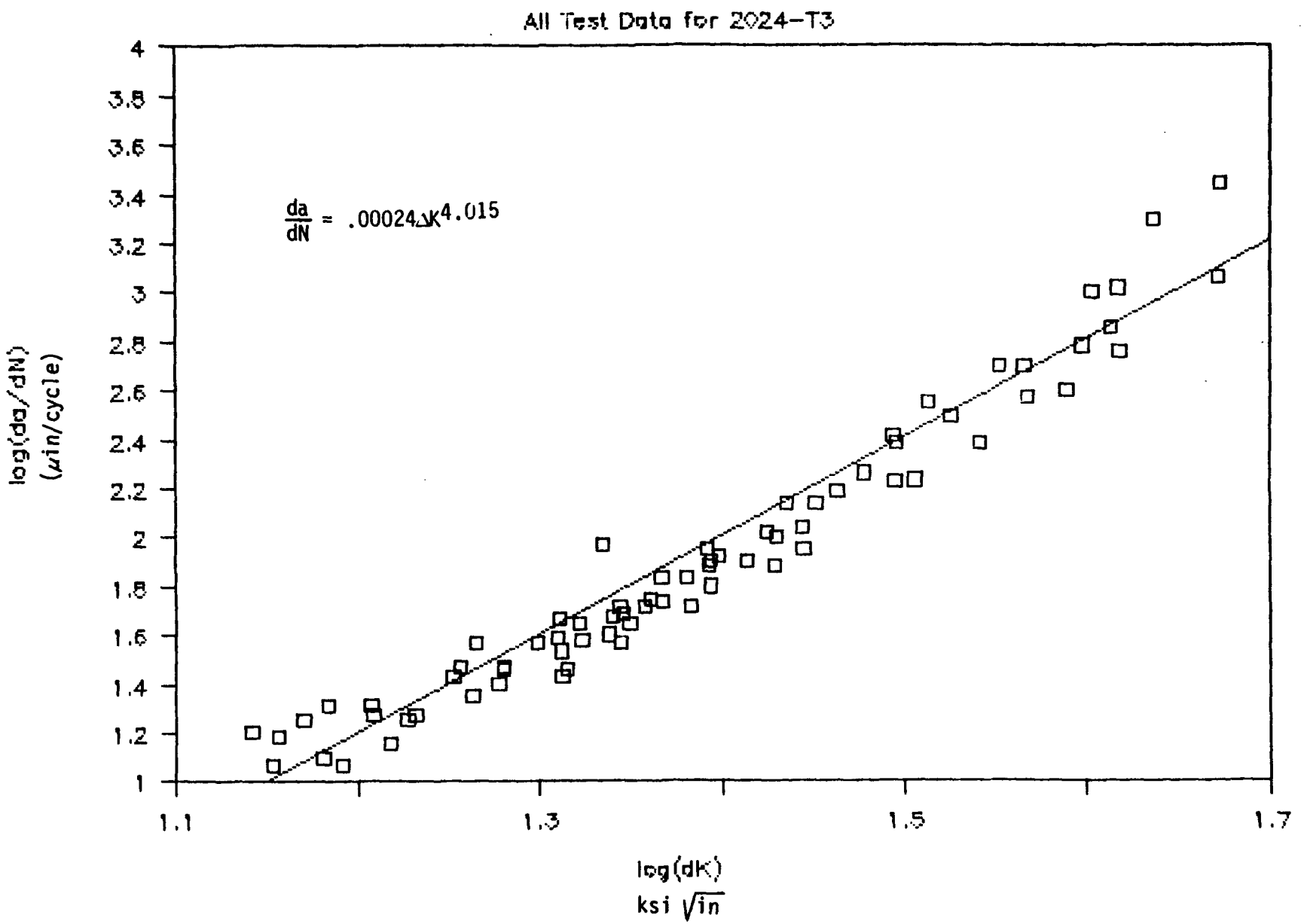

Figure 6-2. Fatigue Life Indicator Tests

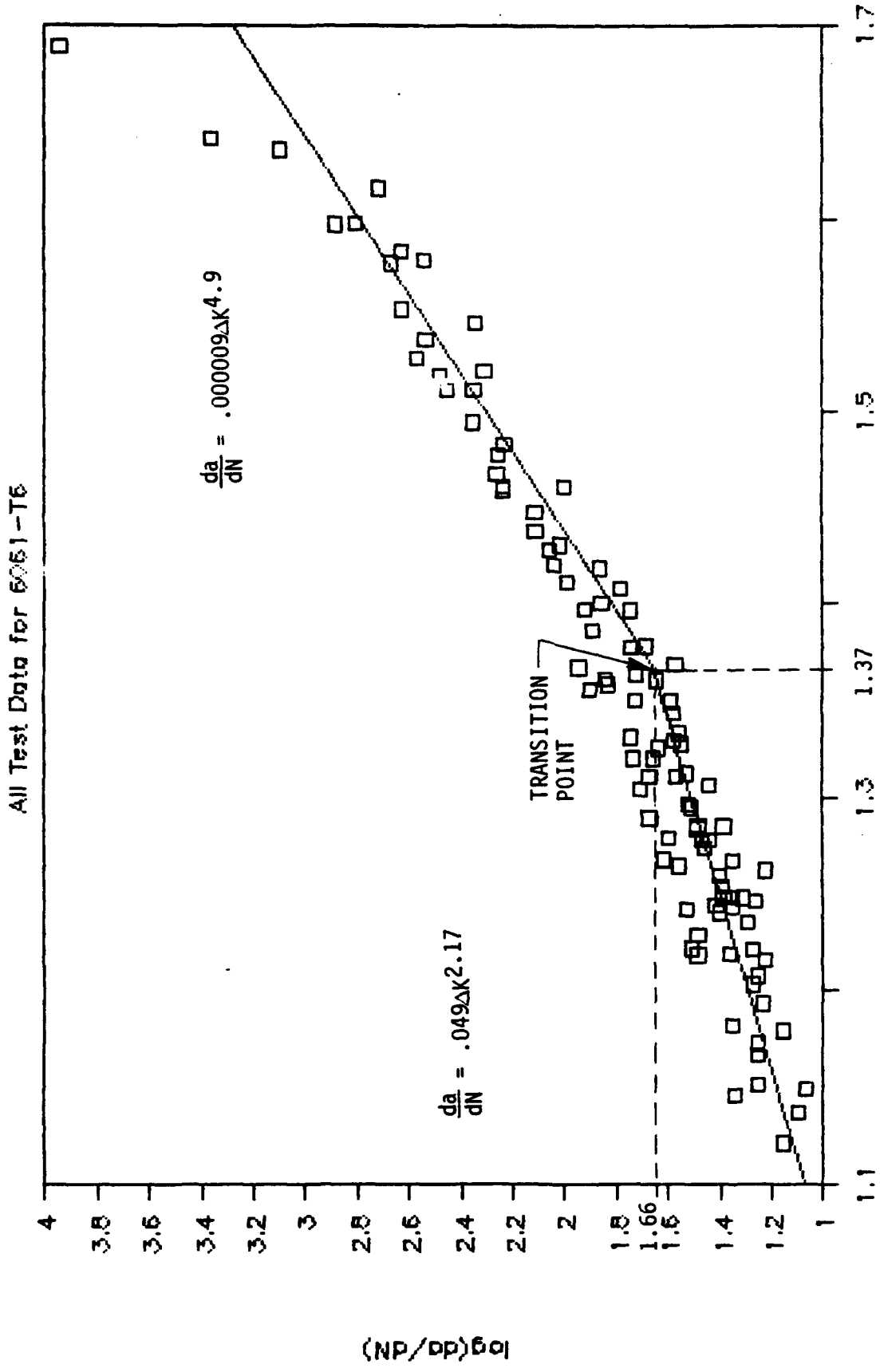

Figure 6-3. Fatigue Life Indicator Tests

The Paris Crack Law predictions for the defined constants and the test data from assemblies E and G are given in Figures 6-4 and 6-5. The constants determined from testing for the 6061-T6 are comparable with the published material constants. Those for the 2024-T3 differ because the published constants are for data with lower crack growth rates.

Table 6-2 gives the computer predicted histograms for these tests. Assemblies E and G show excellent correlation as would be expected since the crack growth constants were derived from these data. However, it is important to note that the two assemblies show very good agreement with each other. This reinforces the repeatability and the predictability of the system.

6.3 Proof-of-Concept Tests

The data from each of the tests was run through the computer program. The results are presented in Table 6-2. Assemblies H and I revealed one additional problem in the development of this system. For these, and all previous assemblies, the coupons were precracked at 24 Ksi. The first 6,000 cycles of these tests were conducted at 20 Ksi. Thus, crack growth was significantly retarded due to the large plastic zone created by the higher stress precracking. However, after 6,000 cycles, the stress level was increased to 25 Ksi. For these cycles, no retardation effects were present and the data correlated well with the computer model. It should be noted that the correlation is poorer in the last 1,500 cycles of Assembly I. As shown in Figure 6-6, the crack growth rate for the 2024-T3 coupon was slower than predicted and the rate for the 6061-T6 coupon was faster than predicted during this period. It is likely that the 2024-T3 coupon began to experience net section yield and thus a disproportionate amount of the applied load was being taken by the 6061-T6 coupon.

Based on the results of Assemblies H and I, the coupons for Assemblies J and K were precracked at 15 Ksi. This stress level was selected because the expected stress level for the AVLB is 17 Ksi based on static test data for a 60 ton crossing. Thus, a pre-cracking level of 15 Ksi should not result in any crack retardation. The test data from Assembly J showed excellent correlation with the computer model for all data from 4,000 cycles onward. Significant crack growth was recorded in both coupons during the first 4,000 cycles thus confirming that the effects of retardation were no longer present. The lack of good correlation of this data to the computer model is due to measurement resolution. At the slow crack growth rates seen in the first 4,000 cycles, it is difficult to accurately measure the small change in the crack length. However, once the cracks grew to about 0.250 in., the measurement system resolution was sufficient and the correlation to the computer model was very good. Only the data after 4,000 cycles is presented in Table 6-2. Assembly K again confirmed that the effects of

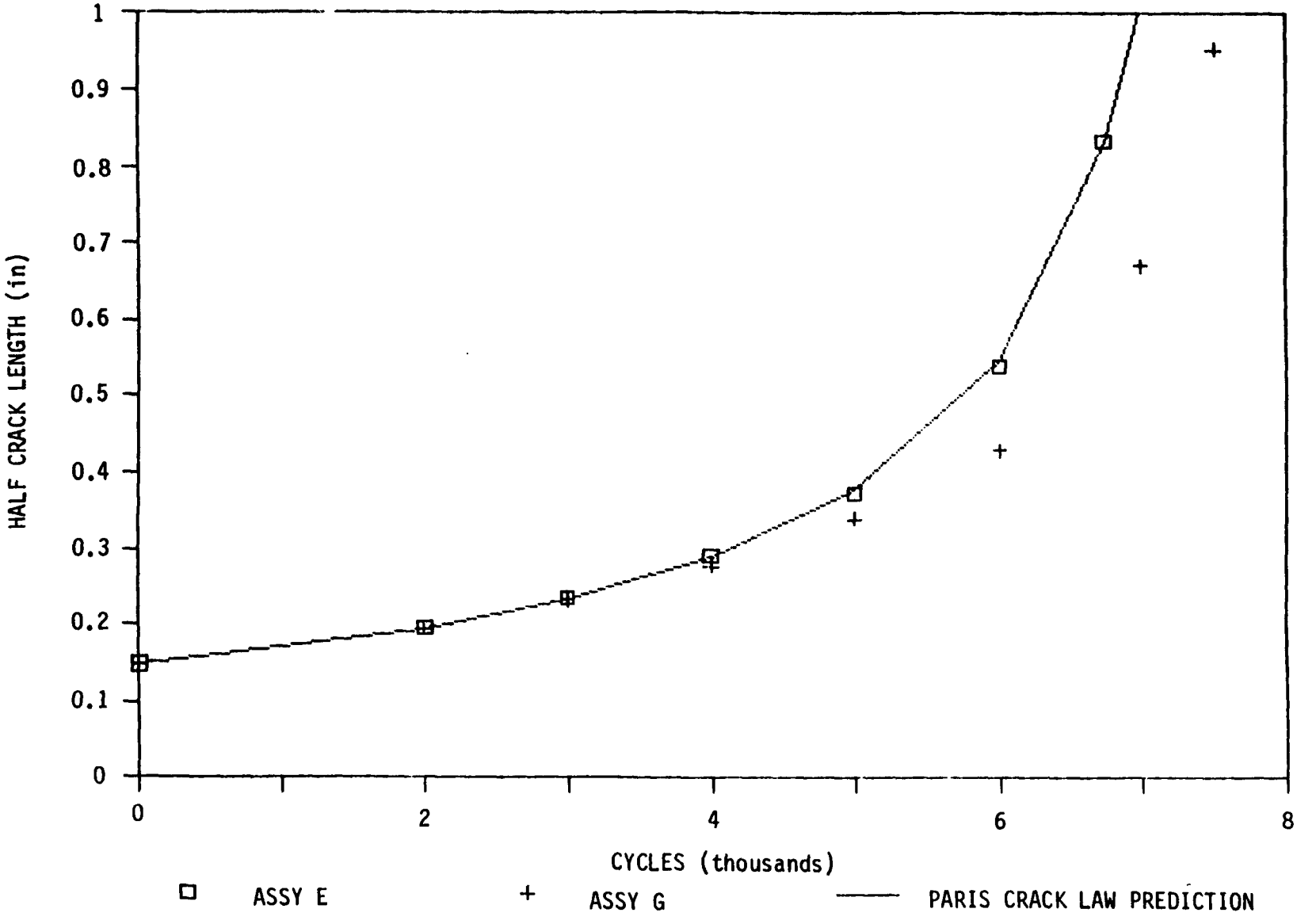

Figure 6-4. Comparison of 2024-T3 Data from Assemblies E and G with Paris Crack Law Prediction

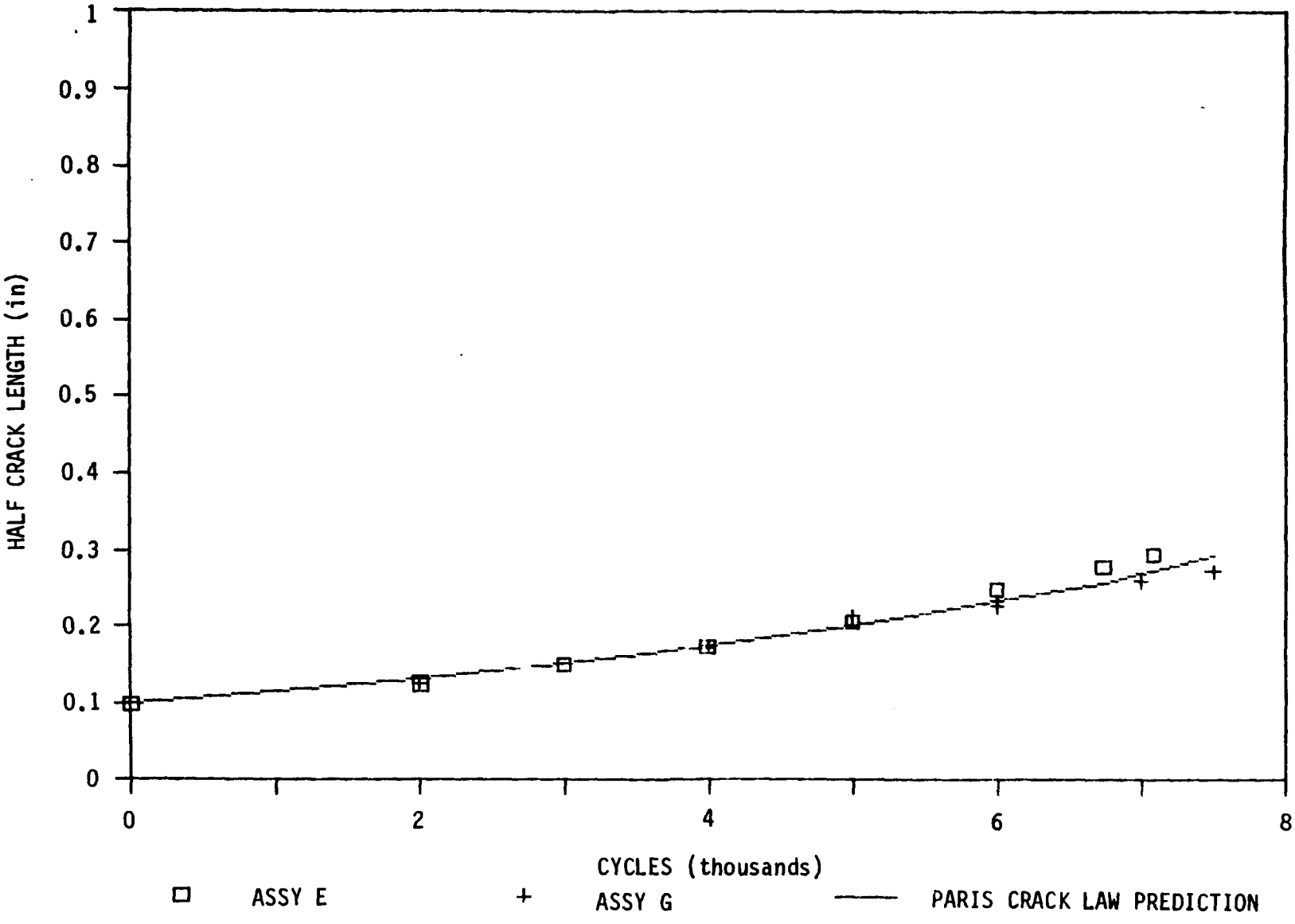

Figure 6-5. Comparison of 6061-T6 Data from Assemblies E and G with Paris Crack Law Prediction

Table 6-2. Test Results versus Predictions

Test Series	Assembly	Test Results Cycles	Test Results Stress (Ksi)	Predictions Cycles	Predictions Stress (Ksi)
II	E	0	24.0		
		2,000	24.0	1,900	23.9
		4,000	24.0	4,000	24.0
		6,000	24.0	7,100	23.0
		6,740	24.0	7,700	23.2
		7,081	24.0	8,000	23.2
	G	0	24.0		
		2,000	24.0	1,900	23.8
		4,000	24.0	4,000	23.7
		6,000	24.0	6,400	23.0
		7,000	24.0	7,100	23.4
		7,500	24.0	7,200	23.8
III	H	0	20.0		
		2,000	20.0		
		4,000	20.0	400	37.1
		6,000	20.0	900	31.9
		0	25.0		
		500	25.0	500	29.5
		1,000	25.0	1,200	26.3
		1,500	25.0	2,300	24.3
		2,000	25.0	2,700	24.8
		2,500	25.0	3,500	24.7
		3,000	25.0	3,800	25.5
	I	0	20.0		
		2,000	20.0		
		4,000	20.0	300	38.0
		6,000	20.0	1,300	29.2
		0	25.0		
		1,000	25.0	1,200	23.6
		1,500	25.0	1,700	23.7
		2,000	25.0	2,400	23.1
		2,500	25.0	3,100	23.2
		3,000	25.0	4,000	22.6
		3,500	25.0	5,900	21.5
		4,000	25.0	6,500	21.9
		4,500	25.0	7,300	22.5

Table 6-2. Test Results versus Predictions (Continued)

Test Series	Assembly	Test Results Cycles	Test Results Stress (Ksi)	Predictions Cycles	Predictions Stress (Ksi)
III	J	0	17.0		
		2,000	17.0	1,500	18.4
		4,000	17.0	3,300	17.8
		5,200	17.0	4,300	17.9
		6,000	17.0	4,700	18.1
		7,000	17.0	5,700	17.9
		8,000	17.0	6,800	17.7
		9,065	17.0	7,900	17.6
		10,000	17.0	8,900	17.4
		11,000	17.0	9,800	17.5
		12,000	17.0	11,000	17.3
		13,000	17.0	12,000	17.3
		14,000	17.0	13,100	17.3
		15,000	17.0	14,400	17.4
	K	0	20.0		
		2,000	20.0	2,200	20.4
		4,000	20.0	4,000	20.0
		6,000	20.0	7,000	18.9

retardation had been eliminated. With a higher applied stress than Assembly J, the crack growth was sufficient for the measurement system resolution and good correlation was achieved for the first 6,000 cycles at 20 Ksi. After 6,000 cycles, the applied stress level was increased to 25 Ksi. At this point, as shown in Figure 6-7, both cracks propagated much faster than predicted.

The stress intensity factor (ΔK) has been defined in Equation 3.2. As the half crack length (a) increases under cyclic loading, the stress intensity factor can increase to a limiting value known as the fracture toughness (Kc) of the material. When ΔK exceeds Kc, fast fracture of the material will begin.

The fracture toughness of 6061-T6 is approximately 30 Ksi $\sqrt{in.}$ (5). This value is exceeded during cycling of Assembly K after 6,000 cycles. Therefore, it is likely that the 6061-T6 coupon was failing faster than would be predicted by the computer model and thus carrying less than its calculated load. Thus, the 2024-T3 coupon was carrying a proportionately higher load. Based on this observation, the computer program is limited to the following maximum ΔK values.

Coupon Material	ΔK max (Ksi $\sqrt{in.}$)
2024-T3	40 (Ref. 4)
6061-T6	30 (Ref. 5)

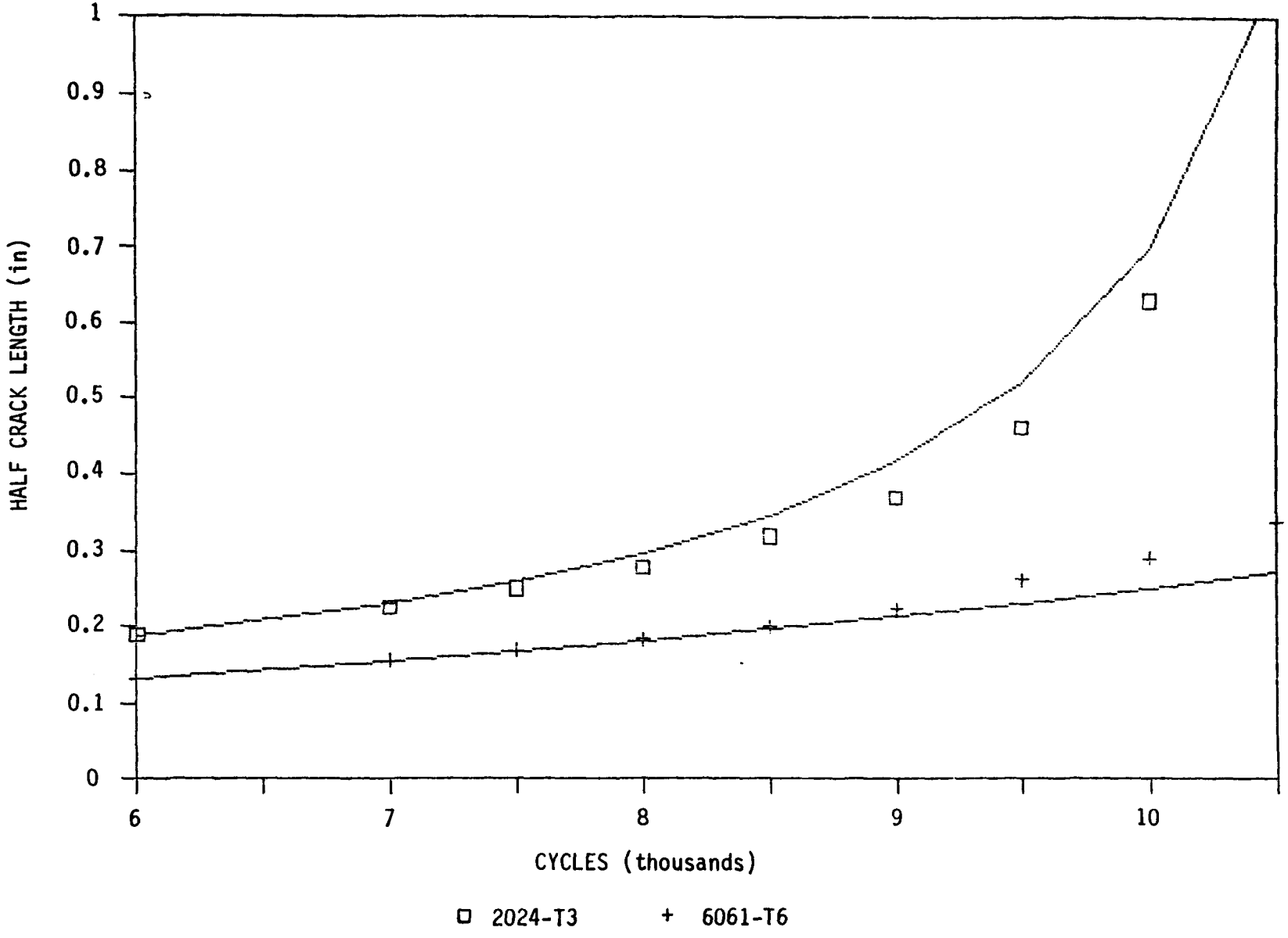

Figure 6-6. Fatigue Life Indicator Assembly I

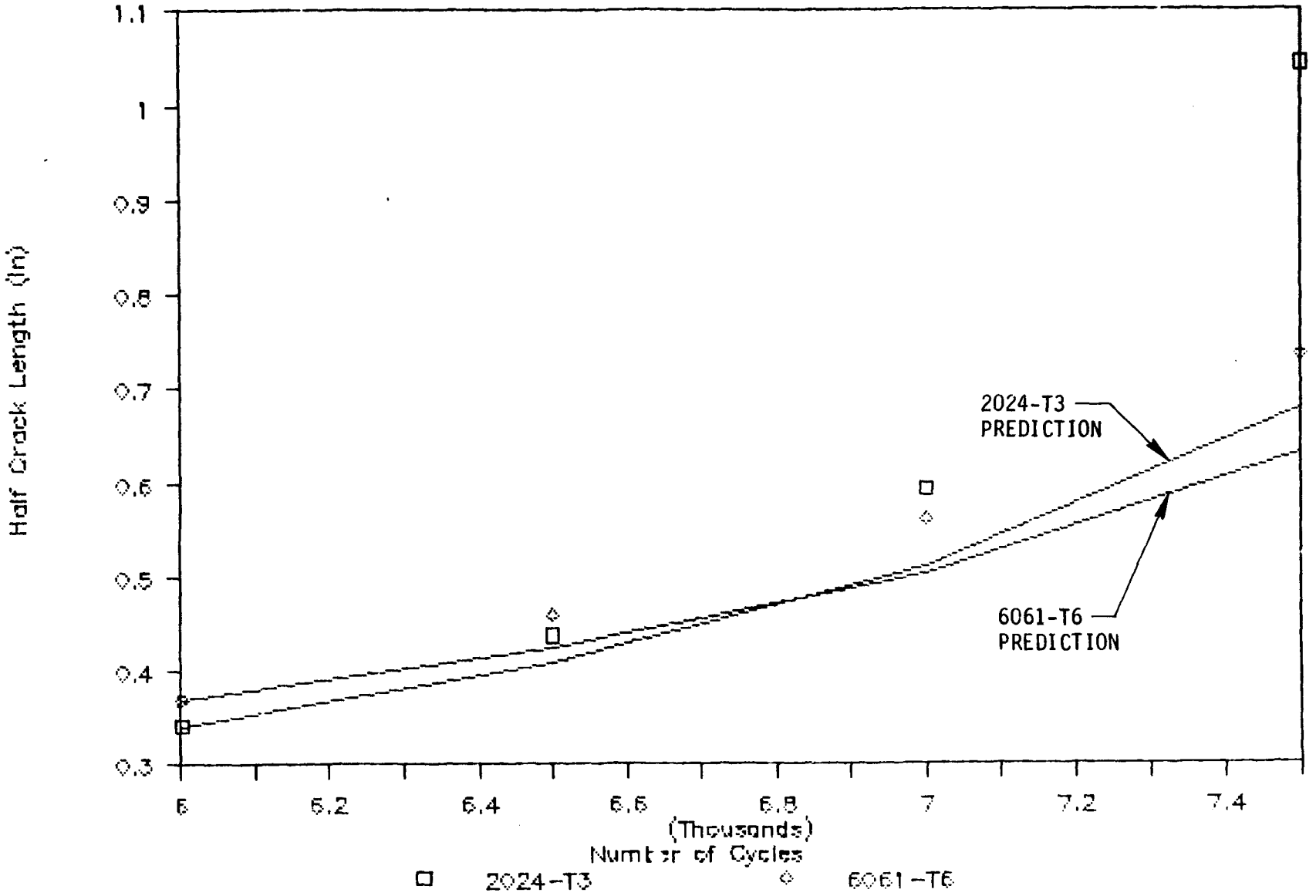

Figure 6-7. Fatigue Life Indicator Assembly K

7. FIELD TESTING

The Fatigue Life Indicator system was developed for use on any mobile army bridge. The field coupons prepared and delivered under this contract were made for use on the Armored Vehicle Launched Bridge (AVLB) described in Section 4. It should be noted that while these coupons were prepared for use on this bridge, they could still be used "as is" on an alternate bridge.

7.1 Field Coupon Attachment

The contract deliverable coupons are 16.5 in. long, 4 in. wide and have an initial half crack length of 0.250 in. For crack growth laws and for the data presented in this report, the half crack length (a) is always used. However, for operator convenience, it should be remembered that the computer program takes the total tip-to-tip crack length as input. Included with these coupons is the necessary attachment hardware. A bolted mechanical joint similar to the one used in the testing is recommended for attachment of the field test coupons. As shown in Figure 7-1, the system will be bolted to the horizontal flange of the tension chord using a 6 bolt pattern and the included aluminum doubler plates. The reduced number of bolts is permissible since the 12 bolt attachment method used in the testing was proven acceptable for much higher stress levels.

7.2 Field Crack Length Measurement

The field measurement of the coupon crack lengths must be done to an accuracy of at least 0.02 in. For the field proof-of-concept, it is recommended that an effort should be made to record these lengths nearly as accurately as in the laboratory. In addition, the errors which would result in general use should be quantified. Therefore, a graduated microscope similar to the one used in the lab should be used for primary measurement during field testing. The recommended general use measurement system is a magnifying glass and a steel scale graduated in hundredths. With this system, it is estimated that the crack length can be measured within 0.02 in. As shown in Figure 3-3, this will limit stress histogram calculation error due to crack measurement error to less than 3 percent.

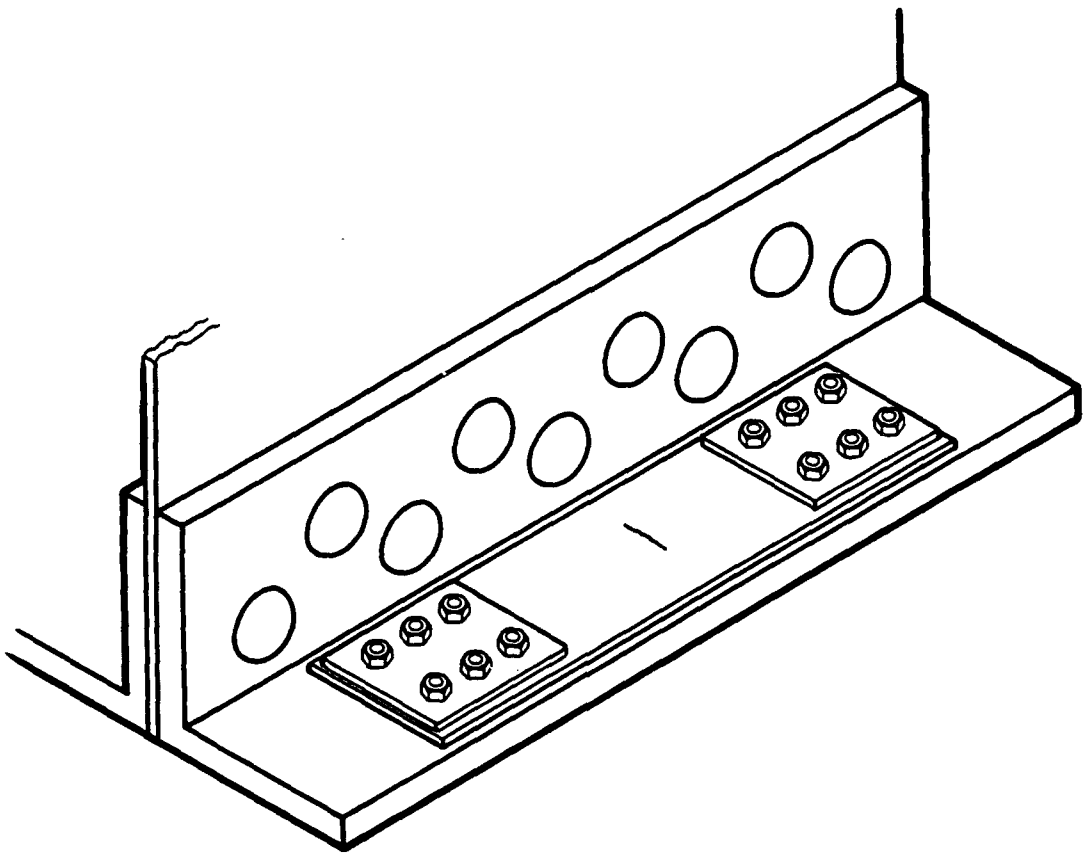

Figure 7-1. Assembly Bolted to AVLB Tension Chord

7.3 Field Protection of the Coupons

The field protection of the coupons will most likely be minimal during the initial system field testing. At this stage, plastic tape is sufficient to protect the cracks from adverse weather and mud. For general use, the coupons will be more completely protected. The crack areas may be covered with plastic tape and then this tape would be further covered by a layer of butyl rubber and a layer of neoprene rubber to provide both moisture and mechanical protection. This protection is commonly used to protect strain gauges and has been found to be very effective with a minimum amount of difficulty of application and removal. In addition, all required materials are commonly commercially available. Alternatively, to allow viewing of the cracks without removal of the cover, a clear plastic cover may be designed to be fit over the crack area. This would permit direct optical reading of the crack lengths without exposure of the cracks to the environment. The edges of the coupons will be covered with a common silicone sealant to prevent moisture from seeping into the cracks from the underside of the coupons.

8. CONCLUSIONS AND RECOMMENDATIONS

The Fatigue Life Indicator (FLI) system provides a valuable tool to monitor the fatigue life of military bridge structures. The concept has been successfully demonstrated in the laboratory. Based on the tests performed several conclusons may be drawn.

- The reliability of the twin coupon method proposed here is due to its dependence on the crack growth rate rather than on crack initiation. The scatter in the growth rate is reasonably small.

- The load histograms (number of cycles and stress levels) can be predicted with reasonable accuracy by monitoring the twin coupon crack lengths. Based on the results shown in Table 6-2, the error in the calculated stress is less than 10 percent. The error in the calculated number of cycles is less than 20 percent. These two sources of error are found to always be opposite in sign. Thus, the error in a Miner cumulative damage calculation will be less than the higher of these two sources of error.

- Pre-cracking of coupons can be consistently carried out on a fatigue machine. It is important to pre-crack the coupons at a stress level below the expected working stress of the applicable bridge at the expected attachment location to avoid any crack growth retardation due to tensile overloading.

- Coupon attachment techniques to the bridge structure need to be finalized. The Huck bolt method was found to be not suitable. Bolted attachment with doubler plates is a viable method in certain cases. A fully bonded method without drilling holes in the parent structure is the most preferred approach. Further testing is required to establish a suitable bonding technique in field conditions.

- Crack length measurement can be achieved to the required accuracy of 0.02 in. using a magnifying lens and a scale graduated in hundredths of an inch. However, the use of an optical method may not be suitable in field conditions due to access limitations.

- A computer program which yields the histograms given the two crack lengths has been developed. This program could be entered on a portable advanced programmable calculator for ease of field use. The load and stress levels computed for each interval of inspection is a "weighted average". This average would be the exact peak stress level if all loading cycles were at the same level. The weighted average will accrue the same fatigue damage as the actual loading during the interval.

- Because of the capability of the system to evaluate load historgrams, the fatigue life in all the critical locations can be determined by employing only one pair of the coupons on the bridge. This is a significant advantage as it provides great flexibility for the coupon attachment locations.

For field validation on the AVLB, several operations are recommended:

- Critical stress locations on the AVLB should be identified by applying strain gages at salient points on the bridge. This work would define the "critical stess profile" of the bridge with strain gage measurements during an AVLB loading test. This information would facilitate identificaiton of a suitable attachment location and also relate the stress at this location to other critical stress locations of the bridge, including those at the hinges.

- Alternative coupon attachment technques should be evlauated. If the recommended technique of bolting to the tension chord proves unacceptable in field testing, alternative techniques should be available. This operation is recommended primarily to aid in the attachment of the Fatique Life Indicator system to bridges other than the AVLB.

- Actual crossing test should be performed with known loading histories to validate the FLI system. To imporve the accuracy and ease of use, two additional operations are recommended.

- A remote crack monitoring system should be evaluated. Although direct optical measurement of the crack lengths is feasible, an electrical system which would allow these measurements to be taken from one end of the bridge would increase accuracy and reduce operator error. In addition, some deployment locations would make access difficult for optical measurement.

- Methods of protecting the FLI system from the environment should be tested in the field. As stated in subsection 9.3, several protection options are available. Additional options would be available if a remote crack length monitoring system permitted the coupons to be permanently sealed. The relative merits of each option should be determined under actual field conditions.

References

1. Fuchs, H.O., R.I. Stephens, "Metal Fatigue in Engineering," John Wiley and Sonse, 1980.

2. Barsom, J.M., S.T. Rolfe, "Fracture and Fatigue Control in Structures," Prentice-Hall, 1987.

3. Broek, D., "Elementary Engineering Fracture Mechanics," Martinus Nijhott Publishers, The Hague, 1983.

4. Hertzberg, R.W., "Deformation and Fracture Mechanics of Engineering Materials," John Wiley and Sons, 1976.

5. Metallic Materials and Elements for Aerospace Vehicle Structures, MIL-HDBK-5D, Chapter 3.

6. Schilling, C.G., K.H. Klippstein, J.M. Barsom and G.T. Blake, "Fatigue of welded Steel Bridge Members under Variable-Amplitude Loadings," National Cooperative Highway Research Program, Report 188, Transportation Research Board, 1978.

7. Fisher, J.W., K.H. Frank, M.A. Hirt, and B.M. McNamee, "Effect of Weldments on the Fatigue Strength of Steel Beams," National Cooperative Highway Research Program, Report 102, Transportation Research Board, 1970.

APPENDIX A
TEST DATA

Fatigue Life Indicator Assembly B, Re-assembled

Reduced Data

Cycles	2a	a	2024-T3 da	dN	da/dN	Est. dSig	dK	Log (da/dN)	Log (dk)
0	0.378	0.189							
1000	0.452	0.226	0.037	1000	36.9	21.85	18.41	1.567	1.265
2100	0.554	0.277	0.051	1100	46.6	21.92	20.45	1.669	1.311
3000	0.626	0.313	0.036	900	40.0	21.96	21.79	1.602	1.338
4100	0.803	0.401	0.088	1100	90.2	22.06	24.77	1.904	1.394
5000	1.001	0.500	0.099	900	110.0	22.17	27.80	2.041	1.444
5500	1.355	0.678	0.177	500	354.6	22.35	32.61	2.550	1.513
5750	1.606	0.803	0.125	250	500.4	22.46	35.68	2.699	1.552
6000	2.122	1.061	0.258	250	1033.2	22.71	41.46	3.014	1.618
6100	2.675	1.337	0.276	100	2763.0	22.98	47.10	3.441	1.673

Cycles	2a	a	6061-T6 da	dN	da/dN	Est.a dSig	dK	Log (da/dN)	Log (dk)
0	0.180	0.090							
1000	0.211	0.105	0.015	1000	15.3	21.85	12.57	1.185	1.099
2100	0.259	0.130	0.024	1100	22.1	21.92	13.98	1.344	1.146
3000	0.292	0.146	0.016	900	18.0	21.96	14.86	1.255	1.172
4100	0.333	0.167	0.021	1100	18.8	22.06	15.95	1.275	1.203
5000	1.394	0.197	0.031	900	34.0	22.17	17.45	1.531	1.242
5500	1.430	0.215	0.018	500	36.0	22.35	18.37	1.556	1.264
5750	1.445	0.222	0.007	250	28.8	22.46	18.77	1.459	1.274
6000	0.468	0.234	0.012	250	46.8	22.71	19.47	1.670	1.289
6100									
6150									
6500	0.524	0.262	0.028	500	55.8	23.62	21.43	1.747	1.331
7000	0.592	0.296	0.034	500	68.4	23.66	22.82	1.835	1.358
7500	0.670	0.335	0.039	500	77.4	23.71	24.31	1.889	1.386
8000	0.779	0.390	0.055	500	109.8	23.77	26.30	2.041	1.420
8500	0.961	0.481	0.091	500	181.8	23.88	29.34	5.203	3.379
9000	1.303	0.652	0.171	500	342.0	24.08	34.45	5.835	3.540
9250	1.683	0.842	0.190	250	759.6	24.31	39.53	6.633	3.677
9325	2.030	1.015	0.174	75	2316.0	24.53	43.80	7.748	3.780
9350	2.471	1.236	0.221	25	8820.0	34.80	48.87	9.085	3.889

Fatigue Life Indicator Assembly C

Reduced Data

			2024-T3			Est.		Log	Log
Cycles	2a	a	da	dN	da/dN	dSig	dK	(da/dN)	(dk)
0	0.256	0.128							
1000	0.286	0.143	0.015	1000	15.3	21.35	14.33	1.185	1.156
2000	0.328	0.164	0.021	1000	20.7	21.29	15.28	1.316	1.184
3000	0.365	0.183	0.019	1000	18.9	21.33	16.16	1.276	1.208
4000	0.401	0.201	0.018	1000	18.0	21.25	16.87	1.255	1.227
5000	0.461	0.230	0.030	1000	29.7	21.19	18.03	1.473	1.256
6000	0.518	0.259	0.029	1000	28.8	21.13	19.06	1.459	1.280
7000	0.596	0.298	0.039	1000	38.7	21.08	20.40	1.588	1.310
8000	0.700	0.350	0.052	1000	52.2	21.06	22.09	1.718	1.344
9000	0.837	0.419	0.068	1000	68.4	20.96	24.03	1.835	1.381
10000	1.111	0.555	0.137	1000	136.8	21.41	28.28	2.136	1.452
10500	1.370	0.685	0.130	500	259.2	21.26	31.18	2.414	1.494
11000	1.868	0.934	0.249	500	498.6	21.50	36.83	2.698	1.566
11200	2.268	1.134	0.200	200	999.0	21.27	40.15	3.000	1.604
11311	2.702	1.351	0.217	111	1954.1	21.02	43.29	3.291	1.636

			6061-T6			Est.		Log	Log
Cycles	2a	a	da	dN	da/dN	dSig	dK	(da/dN)	(dk)
0	0.187	0.094							
1000	0.216	0.108	0.014	1000	14.4	21.35	12.45	1.158	1.095
2000	0.245	0.122	0.014	1000	14.4	21.92	13.21	1.158	1.121
3000	0.281	0.140	0.018	1000	18.0	21.33	14.16	1.255	1.151
4000	0.326	0.163	0.023	1000	22.5	21.25	15.20	1.352	1.182
5000	1.387	0.194	0.031	1000	30.6	21.19	16.52	1.486	1.218
6000	0.439	0.220	0.026	1000	26.1	21.13	17.55	1.417	1.244
7000	0.518	0.259	0.040	1000	39.6	21.08	19.02	1.598	1.279
8000	0.626	0.313	0.054	1000	54.0	21.06	20.89	1.732	1.320
9000	0.765	0.383	0.069	1000	69.3	20.96	22.97	1.841	1.361
10000	0.995	0.498	0.115	1000	115.2	21.41	26.78	2.061	1.428
10500	1.166	0.583	0.086	500	171.0	21.26	28.78	2.233	1.459
11000	1.451	0.725	0.142	500	284.4	21.50	32.46	2.454	1.511
11200	1.598	0.799	0.074	200	369.0	21.27	33.70	2.567	1.528
11300									
11500	2.349	1.175	0.375	300	1251.0	22.48	43.18	3.097	1.635

Fatigue Life Indicator Assembly E

Reduced Data

			2024-T3					Log	Log
Cycles	2a	a	da	dN	da/dN	dSig	dK	(da/dN)	(dk)
0	0.297	0.149							
2000	0.384	0.192	0.043	2000	21.5	24.00	18.64	1.332	1.270
3000	0.472	0.236	0.044	1000	44.0	24.00	20.66	1.644	1.315
4000	0.583	0.292	0.056	1000	55.8	24.00	22.97	1.747	1.361
5000	0.743	0.372	0.080	1000	80.1	24.00	25.93	1.904	1.414
6000	1.080	0.540	0.168	1000	168.3	24.00	31.26	2.226	1.495
6740	1.667	0.833	0.293	740	396.5	24.00	38.83	2.598	1.589
7081	2.441	1.220	0.387	341	1134.9	24.00	46.99	3.055	1.672

			6061-T6					Log	Log
Cycles	2a	a	da	dN	da/dN	dSig	dK	(da/dN)	(dk)
0	0.198	0.099							
2000	0.256	0.128	0.029	2000	14.5	24.00	15.22	1.161	1.182
3000	0.299	0.149	0.021	1000	21.0	24.00	16.44	1.322	1.216
4000	0.347	0.174	0.024	1000	24.3	24.00	17.73	1.386	1.249
5000	0.409	0.204	0.013	1000	30.6	24.00	19.23	1.486	1.284
6000	0.495	0.248	0.043	1000	43.2	24.00	21.16	1.635	1.326
6740	0.553	0.276	0.029	740	38.9	24.00	22.36	1.590	1.349
7081	0.589	0.294	0.018	341	52.8	24.00	23.08	1.723	1.363
7217	0.601	0.301	0.006	136	46.3	24.00	23.32	1.666	1.368

Fatigue Life Indicator Assembly G

Reduced Data

			2024-T3					Log	Log
Cycles	2a	a	da	dN	da/dN	dSig	dK	(da/dN)	(dk)
0	0.295	0.148							
2000	0.396	0.198	0.050	2000	25.2	24.00	18.93	1.401	1.277
3000	0.464	0.232	0.034	1000	34.2	24.00	20.50	1.534	1.312
4000	0.553	0.276	0.044	1000	44.1	24.00	22.36	1.644	1.349
5000	0.679	0.339	0.063	1000	63.0	24.00	24.78	1.799	1.394
6000	0.857	0.428	0.089	1000	89.1	24.00	27.84	1.950	1.445
7000	1.341	0.671	0.242	1000	242.1	24.00	34.83	2.384	1.542
7500	1.908	0.954	0.284	500	567.0	24.00	41.55	2.754	1.619

			6061-T6					Log	Log
Cycles	2a	a	da	dN	da/dN	dSig	dK	(da/dN)	(dk)
0	0.198	0.099							
2000	0.256	0.128	0.029	2000	14.5	24.00	15.22	1.161	1.182
4000	0.344	0.172	0.044	2000	22.0	24.00	17.64	1.342	1.246
6000	0.454	0.227	0.055	2000	27.5	24.00	20.26	1.439	1.307
7000	0.518	0.259	0.032	1000	32.0	24.00	21.65	1.505	1.335
7500	0.544	0.272	0.026	500	52.0	24.00	22.19	1.716	1.346
8000	0.603	0.302	0.030	500	60.0	24.00	23.36	1.778	1.368
9000	0.724	0.362	0.060	1000	60.3	24.00	25.59	1.780	1.408
10000	0.923	0.462	0.100	1000	99.9	24.00	28.90	2.000	1.461
11000	1.364	0.682	0.221	1000	220.5	24.00	35.14	2.343	1.546
11500	1.879	0.940	0.257	500	514.8	24.00	41.23	2.712	1.656

Fatigue Life Indicator Assembly H

Reduced Data

2024-T3

Cycles	2a	a	da	dN	da/dN	dSig	dK	Log (da/dN)	Log (dk)
0	0.261	0.131							
1000	0.277	0.139	0.008	1000	8.1	20.00	13.20	0.908	1.120
2000	0.297	0.149	0.010	1000	9.9	20.00	13.66	0.996	1.135
3000	0.313	0.157	0.008	1000	8.1	20.00	14.03	0.908	1.147
4000	0.347	0.174	0.017	1000	17.1	20.00	14.77	1.233	1.170
5000	0.362	0.181	0.007	1000	7.2	20.00	15.08	0.857	1.178
6000	0.383	0.192	0.011	1000	10.8	20.00	15.52	1.033	1.191
6500	0.477	0.239	0.047	500	93.6	25.00	21.64	1.971	1.335
7000	0.529	0.265	0.026	500	52.22	25.00	22.79	1.718	1.358
7500	0.619	0.310	0.045	500	90.0	25.00	24.66	1.954	1.392
8000	0.756	0.378	0.068	500	136.8	25.00	27.24	2.136	1.435
8500	0.999	0.500	0.122	500	243.0	25.00	31.32	2.386	1.496
9000	1.600	0.800	0.301	500	601.2	25.00	39.64	2.779	1.598

6061-T6

Cycles	2a	a	da	dN	da/dN	dSig	dK	Log (da/dN)	Log (dk)
0	0.196	0.098							
1000	0.205	0.102	0.004	1000	4.5	20.00	11.35	0.653	1.055
2000	0.203	0.120	-0.001	1000	-0.9	20.00	11.30		1.053
3000	0.207	0.104	0.002	1000	1.8	20.00	11.40	0.255	1.057
4000	0.225	0.113	0.009	1000	9.0	20.00	11.89	0.954	1.075
5000	0.239	0.120	0.007	1000	7.2	20.00	11.26	0.857	1.089
6000	0.250	0.125	0.005	1000	5.4	20.00	12.54	0.732	1.098
6500	0.283	0.141	0.016	500	33.4	25.00	16.66	1.511	1.222
7000	0.308	0.154	0.013	500	25.2	25.00	17.38	1.401	1.240
7500	0.349	0.175	0.021	500	41.4	25.00	18.52	1.617	1.268
8000	0.380	0.190	0.015	500	30.6	25.00	19.31	1.486	1.286
8500	0.427	0.213	0.023	500	46.8	25.00	20.46	1.670	1.311
9000	0.464	0.232	0.019	500	37.8	25.00	21.35	1.577	1.329
9500	0.553	0.276	0.044	500	88.2	25.00	23.29	1.945	1.367
10000	0.635	0.318	0.041	500	82.8	25.00	24.98	1.918	1.398
10500	0.765	0.288	0.065	500	129.6	25.00	27.41	2.113	1.438
11000	0.992	0.496	0.113	500	226.8	25.00	31.20	2.356	1.494
11500	1.453	0.726	0.113	500	460.8	25.00	37.76	2.664	1.494

Fatigue Life Indicator Assembly I

Reduced Data

2024-T3

Cycles	2a	a	da	dN	da/dN	dSig	dK	log(da/dN)	log(dk)
0	0.263	0.131							
1000	0.274	0.137	0.005	1000	5.4	20.00	13.11	0.732	1.118
2000	0.283	0.141	0.005	1000	4.5	20.00	13.33	0.653	1.125
3000	0.302	0.151	0.010	1000	9.9	20.00	13.78	0.996	1.139
4000	0.317	0.158	0.007	1000	7.2	20.00	14.11	0.857	1.149
5000	0.358	0.179	0.021	1000	20.7	20.00	15.00	1.316	1.176
6000	0.376	0.188	0.009	1000	9.0	20.00	15.37	0.954	1.187
7000	0.452	0.226	0.038	1000	37.8	25.00	21.06	1.577	1.323
7500	0.500	0.250	0.024	500	48.6	25.00	22.16	1.687	1.346
8000	0.554	0.277	0.027	500	54.0	25.00	23.33	1.732	1.368
8500	0.637	0.319	0.041	500	82.8	25.00	25.01	1.918	1.398
9000	0.738	0.369	0.050	500	100.8	25.00	26.92	2.003	1.430
9500	0.920	0.460	0.091	500	181.8	25.00	30.05	2.260	1.478
10000	1.258	0.629	0.169	500	338.0	25.00	35.14	2.529	1.546
10500	3.000	1.500	0.871	500	1742.0	25.00	54.27	3.241	1.735

6061-T6

Cycles	2a	a	da	dN	da/dN	dSig	dK	log(da/dN)	log(dk)
0	0.202	0.101							
1000	0.203	0.102	0.001	1000	0.9	20.00	11.30	-0.046	1.053
2000	0.205	0.103	0.001	1000	0.9	20.00	11.35	-0.046	1.055
3000	0.214	0.107	0.005	1000	4.5	20.00	11.60	0.653	1.064
4000	0.221	0.111	0.004	1000	3.6	20.00	11.79	0.556	1.072
5000	0.239	0.120	0.009	1000	9.0	20.00	12.26	0.954	1.089
6000	0.266	0.133	0.014	1000	13.5	20.00	12.94	1.130	1.112
7000	0.311	0.156	0.022	1000	22.5	25.00	17.48	1.352	1.243
7500	0.337	0.168	0.013	500	25.2	25.00	18.18	1.401	1.260
8000	0.366	0.183	0.015	500	29.7	25.00	18.96	1.473	1.278
8500	0.400	0.200	0.017	500	33.3	25.00	19.81	1.522	1.297
9000	0.445	0.222	0.022	500	45.0	25.00	20.89	1.653	1.320
9500	0.524	0.262	0.040	500	79.2	25.00	22.68	1.899	1.356
10000	0.580	0.290	0.028	500	55.8	25.00	23.85	1.747	1.378
10500	0.677	0.338	0.049	500	97.2	25.00	25.78	1.988	1.411
11000	0.850	0.425	0.086	500	172.8	25.00	28.88	2.238	1.461
11500	1.073	0.536	0.112	500	223.2	25.00	32.45	2.349	1.511
12000	1.496	0.748	0.212	500	423.0	25.00	38.32	2.626	1.583

Fatigue Life Indicator Assembly J

Reduced Data

2024-T3

Cycles	2a	a	da	dN	da/dN	dSig	dK	log(da/dN)	log(dk)
0	0.391	0.195							
1000	0.423	0.212	0.016	1000	16.2	17.00	13.86	1.210	1.142
2000	0.446	0.223	0.012	1000	11.7	17.00	14.24	1.068	1.153
3000	0.482	0.241	0.018	1000	18.0	17.00	14.80	1.255	1.170
4000	0.508	0.254	0.013	1000	12.6	17.00	15.18	1.100	1.181
5000	0.531	0.266	0.012	1000	11.7	17.00	15.53	1.068	1.191
6000	0.572	0.286	0.021	1000	20.7	17.00	16.12	1.316	1.207
7000	0.601	0.301	0.014	1000	14.4	17.00	16.52	1.158	1.218
8000	0.639	0.320	0.019	1000	18.9	17.00	17.03	1.276	1.231
9200	0.704	0.352	0.032	1200	27.0	17.00	17.87	1.431	1.252
10000	0.740	0.370	0.018	800	22.5	17.00	18.33	1.352	1.263
11000	0.799	0.400	0.030	1000	29.7	17.00	19.05	1.473	1.280
12000	0.873	0.437	0.037	1000	36.9	17.00	19.91	1.567	1.299
13065	0.968	0.484	0.048	1065	44.8	17.00	20.97	1.651	1.322
14000	1.057	0.528	0.044	935	47.2	17.00	21.90	1.674	1.340
15000	1.193	0.597	0.068	1000	68.4	17.00	23.28	1.835	1.367
16000	1.345	0.672	0.076	1000	75.6	17.00	24.71	1.879	1.393
17000	1.553	0.777	0.104	1000	104.4	17.00	26.56	2.019	1.424
18000	1.859	0.930	0.153	1000	153.0	17.00	29.05	2.185	1.463
19000	2.479	1.239	0.310	1000	309.6	17.00	33.54	2.491	1.526

6061-T6

Cycles	2a	a	da	dN	da/dN	dSig	dK	log(da/dN)	log(dk)
0	0.389	0.194							
1000	0.414	0.207	0.013	1000	12.6	17.00	13.71	1.100	1.137
2000	0.437	0.219	0.012	1000	11.7	17.00	14.09	1.068	1.149
3000	0.473	0.237	0.018	1000	18.0	17.00	14.66	1.255	1.166
4000	0.502	0.251	0.014	1000	14.4	17.00	15.10	1.158	1.179
5000	0.536	0.268	0.017	1000	17.1	17.00	15.60	1.233	1.193
6000	0.572	0.286	0.018	1000	18.0	17.00	16.12	1.255	1.207
7000	0.610	0.305	0.019	1000	18.9	17.00	16.64	1.276	1.221
8000	0.650	0.325	0.020	1000	19.8	17.00	17.18	1.297	1.235
9200	0.709	0.355	0.030	1200	27.8	17.00	17.94	1.394	1.254
10000	0.736	0.368	0.014	800	16.9	17.00	18.28	1.227	1.262
11000	0.792	0.396	0.028	1000	27.9	17.00	18.96	1.446	1.278
12000	0.857	0.428	0.032	1000	32.4	17.00	19.72	1.511	1.295
13065	0.929	0.464	0.036	1065	33.8	17.00	20.53	1.529	1.312
14000	0.995	0.498	0.033	935	35.6	17.00	21.26	1.552	1.328
15000	1.071	0.536	0.038	1000	37.8	17.00	22.05	1.577	1.343
16000	1.159	0.580	0.044	1000	44.1	17.00	22.94	1.644	1.361
17000	1.256	0.628	0.049	1000	48.9	17.00	23.88	1.687	1.378
18000	1.368	0.684	0.056	1000	55.8	17.00	24.92	1.747	1.397
19000	1.514	0.757	0.073	1000	72.9	17.00	26.21	1.863	1.419

Fatigue Life Indicator Assembly K

Reduced Data

2024-T3

Cycles	2a	a	da	dN	da/dN	dSig	dK	log(da/dN)	log(dk)
0	0.391	0.195							
1000	0.436	0.218	0.022	1000	22.5	20.00	16.54	1.352	1.219
2000	0.479	0.239	0.022	1000	21.6	20.00	17.34	1.334	1.239
3000	0.524	0.262	0.023	1000	22.5	20.00	18.14	1.352	1.259
4000	0.565	0.283	0.021	1000	20.7	20.00	18.84	1.316	1.275
5000	0.612	0.306	0.023	1000	23.4	20.00	19.61	1.369	1.292
6000	0.682	0.341	0.035	1000	35.1	20.00	20.70	1.545	1.316
6500	0.873	0.437	0.095	500	190.8	25.00	29.28	2.281	1.467
7000	1.186	0.593	0.157	500	313.2	25.00	34.13	2.496	1.533
7500	2.088	1.004	0.451	500	901.8	25.00	45.28	2.955	1.656

6061-T6

Cycles	2a	a	da	dN	da/dN	dSig	dK	log(da/dN)	log(dk)
0	0.396	0.198							
1000	0.457	0.229	0.031	1000	30.6	20.00	16.95	1.486	1.229
2000	0.499	0.249	0.021	1000	20.7	20.00	17.70	1.316	1.248
3000	0.544	0.272	0.022	1000	22.5	20.00	18.48	1.352	1.267
4000	0.592	0.296	0.024	1000	24.3	20.00	19.29	1.386	1.285
5000	0.666	0.333	0.037	1000	36.9	20.00	20.46	1.567	1.311
6000	0.738	0.369	0.036	1000	36.0	20.00	21.53	1.556	1.333
6500	0.918	0.450	0.090	500	180.0	25.00	30.02	2.255	1.477
7000	1.121	0.561	0.102	500	203.4	25.00	33.18	2.308	1.521
7500	1.467	0.734	0.173	500	345.6	25.00	37.95	2.539	1.579

APPENDIX B
FMFLCALC
COMPUTER PROGRAM

```
10 '  PROGRAM FMFLCALC.BAS
20 '
30 ' FLI STRESS AND CYCLES CALCULATION PROGRAM
40 '
50 ' D. THOMSON  FOSTER-MILLER INC. 28 SEP 90
60 '
70 ' ************************************************************************
80 A1I=.25
90 A2I=.25
100 WW=0
110 CLS
120 PRINT"            TWIN COUPON BRIDGE FATIGUE LIFE INDICATOR"
130 PRINT
140 PRINT"         Developed for the US Army Troop Support Command"
150 PRINT
160 PRINT
170 PRINT"This program will determine the mean applied stress and number of"
180 PRINT"cycles experienced by the twin coupon bridge fatigue life indicator"
190 PRINT
200 PRINT"Analysis Options:
210 PRINT"A. The mean stress and total cycles applied since"
220 PRINT"   installation of the system."
230 PRINT"       Data Required:"
240 PRINT"           1. Current 2024-T3 coupon crack length (Inches)"
250 PRINT"           2. Current 6061-T6 coupon crack length (Inches)"
260 PRINT
270 PRINT"B. The mean stress and cycles applied over some increment of"
280 PRINT"   the life of the system."
290 PRINT"       Data Required:"
300 PRINT"           3. Initial 2024-T3 coupon crack length (Inches)"
310 PRINT"           4. Initial 6061-T6 coupon crack length (Inches)"
320 PRINT"           3. Current 2024-T3 coupon crack length (Inches)"
330 PRINT"           4. Current 6061-T6 coupon crack length (Inches)"
340 PRINT
350 INPUT"Input the desired analysis option (A/B)";A$
360 CLS
370 IF A$<>"b" THEN 450
380 PRINT
390 PRINT
400 INPUT"Enter the Initial Tip-to-Tip Crack Length for 2024-T3";A1I
410 PRINT
420 INPUT"Enter the Initial Tip-to-Tip Crack Length for 6061-T6";A2I
430 A1I=A1I/2
440 A2I=A2I/2
450 PRINT
460 PRINT
470 ON ERROR GOTO 1650
480 IND=0
490 NN=1
500 PI=3.14159
510 ' PARIS CRACK GROWTH CONSTANTS
520 '  2024-T3   LINEAR FIT
530 E11=4.015
540 C11=.00024
550 '
560 '  6061-T6  BI-LINEAR FIT
570 E21=2.17
580 C21=.049
590 E22=4.9
600 C22=9.000001E-06
```

```
610 PRINT
620 TOL=.05
630 PRINT
640 PRINT
650 PRINT
660 INPUT"Enter the Current Tip-to-Tip Crack Length for 2024-T3";A1
670 PRINT
680 INPUT"Enter the Current Tip-to-Tip Crack Length for 6061-T6";A2
690 IF A1>3.5 OR A2>2 THEN 1720
700 IF A1<A1I OR A2<A2I THEN 1650
710 A1=A1/2
720 A2=A2/2
730 '
740 ' BEGIN CALCULATIONS
750 '
760 EX1=1-E11/2
770 EX2=1-E21/2
780 EX4=1-E22/2
790 '
800 '
810 ' CASE I
820 '
830 '
840 K1=C11*EX1*PI^(E11/2)
850 K2=C21*EX2*PI^(E21/2)
860 DA1=A1^EX1-A1I^EX1
870 DA2=A2^EX2-A2I^EX2
880 SIG1=((K2*DA1)/(K1*DA2))^(1/(E11-E21))
890 SIG1ORIG=SIG1
900 N=DA1/(K1*SIG1^E11)
910 '
920 'check if da2/dn is beyond transition
930 '
940 ATR2=((C21*SIG1^E21*PI^(E21/2))/(C22*SIG1^E22*PI^(E22/2)))^(2/(E22-E21))
950 IF A2>ATR2 THEN 970
960 GOTO 1430
970 ' CASE III
980 '
990 '
1000 'Find When da2/dN is at transition
1010 '
1020 IF SIG1>50 THEN GOTO 1650
1030 A2200=((C21*SIG1^E21*PI^(E21/2))/(C22*SIG1^E22*PI^(E22/2)))^(2/(E22-E21))
1040 DD2=C21*SIG1^E21*PI^(E21/2)*EX2
1050 N200=(A2200^EX2-A2I^EX2)/DD2
1060 '
1070 'Find a1 when da2/dN is at transition
1080 '
1090 DD1=C11*SIG1^E11*PI^(E11/2)*EX1
1100 A1200=((N200*DD1)+A1I^EX1)^(1/EX1)
1110 IF A2200<=A2 THEN 1190
1120 IF IND=0 THEN 1150
1130 SIG1=SIG1*(1+TOL/10)
1140 GOTO 970
1150 SIG1=SIG1ORIG*(1+NN*TOL)
1160 NN=NN+1
1170 GOTO 970
1180 '
1190 'Solve for Stress for Case III
1200 '
```

```
1210 K1=C11*EX1*PI^(E11/2)
1220 K2=C22*EX4*PI^(E22/2)
1230 DA1=A1^EX1-A1200^EX1
1240 DA2=A2^EX4-A2200^EX4
1250 SIG3=((K2*DA1)/(K1*DA2))^(1/(E11-E22))
1260 N2B=DA2/(K2*SIG3^E22)
1270 N=N200+N2B
1280 CLS
1290 WW=WW+1
1300 LOCATE 10,20
1310 PRINT"ITERATION ";WW
1320 IF ABS((SIG3-SIG1)/SIG1)<=TOL THEN 1430
1330 IF SIG3<SIG1 AND IND=0 THEN 1400
1340 IF SIG3<SIG1 AND IND=1 THEN 1380
1350 SIG1=SIG1*(1-TOL)
1360 IND=1
1370 GOTO 970
1380 SIG1=SIG1*(1+TOL/10)
1390 GOTO 970
1400 SIG1=(SIG1+SIG3)/2
1410 GOTO 970
1420 '
1430 'print out results
1440 '
1450 CLS
1460 PRINT
1470 PRINT
1480 PRINT
1490 PRINT"                FATIGUE LIFE INDICATOR"
1500 PRINT"              Stress Cycle Calculation"
1510 PRINT
1520 PRINT
1530 PRINT
1540 PRINT"     Mean Applied Stress in KSI = ";INT((SIG1*10)+.5)/10
1550 PRINT
1560 PRINT
1570 PRINT"     Number of Cycles = ";INT((N*10000)+.5)*100
1580 PRINT
1590 PRINT
1600 PRINT
1610 PRINT
1620 PRINT
1630 PRINT
1640 END
1650 CLS
1660 LOCATE 10,5
1670 PRINT"The crack lengths entered do not yeild a solution"
1680 PRINT
1690 PRINT
1700 PRINT
1710 END
1720 CLS
1730 LOCATE 10,1
1740 PRINT"The crack lengths entered exceed the useful life of the"
1750 PRINT"            Fatigue Life Indicator system."
1760 PRINT
1770 PRINT
1780 PRINT
1790 END
```

APPENDIX C
SAMPLE CALCULATION

Sample Calculation of Stress Histogram

Assembly J after 12,000 cycles

$a_{i\ 2024\text{-}T3}$	= 0.254	$a_{i\ 6061\text{-}T6}$	= 0.251
$a_{\ 2024\text{-}T3}$	= 0.672	$a_{\ 6061\text{-}T6}$	= 0.580

Using:	2024-T3	6061-T6
	$C_1 = 2.4E\text{-}4$	$C_2 = 4.9E\text{-}2$
	$n_1 = 4.015$	$n_2 = 2.17$
		$C_3 = 9.0E\text{-}6$
		$n_3 = 4.90$

From Equation 3-7:

$$\Delta\sigma_1 = 17.31 \text{ Ksi}$$

From the following equation:

$$a_{TR} = \left[\frac{C_2 \, \Delta\sigma^{n_2} \, \pi^{\frac{n_2}{2}}}{C_3 \, \Delta\sigma^{n_3} \, \pi^{\frac{n_3}{2}}} \right]^{\frac{2}{n_3 - n_2}}$$

$a_{6061\text{-}T6} = 0.5795$ at transition

From equation 3-5:

$N = 11000$ at transition

From the following equation:

$$a = \left[\left[NC_1 \, \Delta\sigma^{n_1} \, \pi^{\frac{n_1}{2}} \left(1 - \frac{n_1}{2}\right) \right] + a_i^{1 - \frac{n_1}{2}} \right]^{\frac{1}{1 - \frac{n_1}{2}}}$$

$a_{2024\text{-}T6} = 0.6702$ at transition

From equation 3-7 above transition where C_3 and n_3 replace C_2 and n_2 respectively and:

$a_{i\ 2024\text{-}T3} = a_{TR} = 0.6702$
$a_{i\ 6061\text{-}T6} = a_{TR} = 0.5795$

$\Delta\sigma_2 = 17.30$ Ksi above transition

Since $\Delta\sigma_1$ and $\Delta\sigma_2$ agree within 5 percent, the calculation is complete.

From equation 3-5:

N = 10 above transition

Final program results:

$\Delta\sigma = 17.3$ Ksi
N = 11000 cycles

APPENDIX D
COUPON ATTACHMENT PROCEDURE

FLI COUPON PREPARATION AND MOUNTING

- Clamp coupon lengthwise to top horizontal surface of tension chord (keep coupon parallel to edge of flange)
- Clamp doubler plates over ends of coupon and drill through with 1/4 in. drill bit
- Mark doubler plates and coupon to maintain location and orientation
- Unclamp doubler plates and coupon
- Enlarge coupon holes with 9/32 in. drill bit
- Deburr drilled holes in coupon and tension chord with a large drill bit
- Sand all mating surfaces with 100 grit sandpaper. Sanding direction is across the coupon
- Degrease all mating surfaces with acetone
- Remove protective tape from underside of coupon
- Bolt coupon and doubler plates to tension chord, at marked location and orientation, using 1/4-20 bolts. Do not tighten
- Clamp coupon down flat against tension chord
- Torque bolts to 18 ft-lb
- Unclamp coupon.